Gut Microbe-Derived Trimethylamine Shapes Circadian Rhythms Through the Host Receptor TAAR5.

Kala K. Mahen[1-3], William J. Massey[2,4], Danny Orabi[1], Amanda L. Brown[1], Thomas C. Jaramillo[5], Amy C. Burrows[1], Anthony J. Horak III[1], Sumita Dutta[1,2], Marko Mrdjen[1-4], Nour Mouannes[1-3], Venkateshwari Varadharajan[1,2], Lucas J. Osborn[1-3], Xiayan Ye[1], Dante M. Yarbrough[1], Treg Grubb[1], Natalie Zajczenko[1], Rachel Hohe[1-3], Rakhee Banerjee[1], Pranavi Linga[1], Dev Laungani[1], Adeline M. Hajjar[2,7], Naseer Sangwan[2,6], Mohammed Dwidar[2,7], Jennifer A. Buffa[2,7], Garth R. Swanson[8], Zeneng Wang[2,7], and J. Mark Brown[1-3*]

[1]Department of Cancer Biology, Cleveland Clinic, Cleveland, OH 44195, USA
[2]Center for Microbiome and Human Health, Lerner Research Institute of the Cleveland Clinic; Cleveland, OH, USA.
[3]Department of Molecular Medicine, Cleveland Clinic Lerner College of Medicine of Case Western Reserve University; Cleveland, Ohio, USA.
[4]Department of Inflammation and Immunity, Cleveland Clinic, Cleveland, OH 44195, USA
[5]Rodent Behavior Core, Lerner Research Institute, Cleveland Clinic, Cleveland, Ohio, USA
[6]Microbial Sequencing & Analytics Core Facility, Cleveland Clinic, Lerner Research Institute, Cleveland, OH 44195, USA
[7]Department of Cardiovascular and Metabolic Sciences, Cleveland Clinic, Lerner Research Institute, Cleveland, OH 44195, USA
[8]Department of Medicine, Medical University of South Carolina, Charleston, SC 29425, USA
[*]To whom correspondence should be addressed: Department of Cancer Biology, Cleveland Clinic, Cleveland, OH 44195, USA
Tel: 216-444-8340; Fax: 216-444-9404; E-mail: brownm5@ccf.org

Running Title: TMA-TAAR5 Signaling Impacts Host Circadian Rhythms

Keywords: Microbiome, Circadian, Metabolism, Olfaction

Abstract

Elevated levels of the gut microbe-derived metabolite trimethylamine N-oxide (TMAO) are associated with cardiometabolic disease risk. However, the mechanism(s) linking TMAO production to human disease are incompletely understood. Initiation of the metaorganismal TMAO pathway begins when dietary choline and related metabolites are converted to trimethylamine (TMA) by gut bacteria. Gut microbe-derived TMA can then be further oxidized by host flavin-containing monooxygenases to generate TMAO. Previously, we showed that drugs lowering both TMA and TMAO protect mice against obesity via rewiring of host circadian rhythms. Although most mechanistic studies in the literature have focused on the metabolic end product TMAO, here we have instead tested whether the primary metabolite TMA alters host metabolic homeostasis and circadian rhythms via trace amine-associated receptor 5 (TAAR5). Remarkably, mice lacking the host TMA receptor (*Taar5*$^{-/-}$) have altered circadian rhythms in gene expression, metabolic hormones, gut microbiome composition, and innate behaviors. In parallel, mice genetically lacking bacterial TMA production or host TMA oxidation have altered circadian rhythms. These results provide new insights into diet-microbe-host interactions relevant to cardiometabolic disease.

Introduction

Modern investigation into human disease relies heavily on genetic and genomic approaches, and most assume that human disease is primarily driven by variation in the human genome. However, in the post genomic era we now understand that human genetic variation explains only a small proportion of risk for complex diseases such as obesity, diabetes, and cardiovascular disease (CVD). Instead, in many cases environmental factors are the predominant drivers of cardiometabolic disease pathogenesis. Among all contributing environmental factors, it is clear that dietary patterns, and diet-driven alterations in the gut microbiome, can profoundly impact many common human diseases.[1-4] There are now many examples of diet-microbe-host interactions shaping human disease, but one of the more compelling is the reproducible link between elevated trimethylamine N-oxide (TMAO) levels and cardiovascular disease (CVD) risk.[5-12] TMAO is generated by a metaorganismal (*i.e.* microbe & host) pathway where dietary substrates such as choline, *L*-carnitine, and γ-butyrobetaine are metabolized by gut microbial enzymes to generate the primary metabolite trimethylamine (TMA).[5-12] TMA is then further metabolized by the host enzyme flavin-containing monooxygenase 3 (FMO3) in the liver to produce trimethylamine-N-oxide (TMAO).[10] Elevated TMAO levels are associated with many human diseases including diverse forms of CVD[5-12], obesity[13,14], type 2 diabetes[15,16], chronic kidney disease (CKD)[17,18], neurodegenerative conditions including Parkinson's and Alzheimer's disease[19,20], and several cancers[21,22]. Many of these disease associations have been validated in several large population meta-analyses[23-25] and Mendelian randomization studies[26,27]. The emerging body of evidence supports the notion that elevated TMAO levels are causally related to cardiometabolic disease pathogenesis. In further support, therapies aimed at lowering circulating TMAO levels provide striking protection

against cardiometabolic disease in animal models[28-36]. Several independent studies have now shown that inhibition of either the host TMAO-producing enzyme FMO3 or the microbial TMA-producing enzyme CutC protects against diet-induced atherosclerosis[15,30], heart failure[32], thrombosis[29,31], obesity[13,33], liver disease[34], insulin resistance[13,33], CKD[35,36], and abdominal aortic aneurysm[37].

Even though TMAO lowering therapies are very effective in preclinical animal models, the underlying mechanism(s) linking the metaorganismal production of TMAO to cardiometabolic disease pathogenesis are still incompletely understood. There is some evidence that TMAO can promote inflammatory processes via activation of the nucleotide-binding domain, leucine-rich-containing family, pyrin domain-containing-3 (NLRP3) inflammasome and nuclear factor κB (NFκB).[38-41] TMAO can also activate the endoplasmic reticulum (ER) stress kinase PERK (EIF2AK3) in hepatocytes to promote metabolic disturbance.[28] In parallel, TMAO promotes stimulus-dependent calcium release in platelets to promote thrombosis.[8] Although the end product of the pathway TMAO clearly impacts cell signaling in the host to impact cardiometabolic disease, these TMAO-driven mechanisms do not fully explain how elevated TMAO levels contribute to so many diverse diseases in humans. In addition to TMAO-driven signaling mechanisms, we recently reported that major components of the TMAO pathway (choline, TMA, FMO3, and TAAR5) oscillate in a highly circadian fashion.[33] Furthermore, gut microbe-targeted drugs that selectively block TMA production alter host circadian rhythms in the gut microbiome and host phospholipid metabolism.[33] It is important to note that disruption of the circadian clock is a common hallmark of almost all diseases where TMAO levels are elevated[42-45]. To follow up on the potential links between the TMAO pathway and host circadian disruption here we have used genetic knockout approaches at the level of gut microbial TMA production (i.e. *cutC*-null microbial communities), host TMA oxidation (i.e. *Fmo3*$^{-/-}$), or host sensing of TMA (i.e. *Taar5*$^{-/-}$).

Results here further bolster the concept that TMA-driven TAAR5 activation shapes host circadian rhythms.

Results

Mice Lacking the TMA Receptor TAAR5 Have Altered Circadian Rhythms in Metabolic Homeostasis and Innate Olfactory-Related Behaviors

We recently demonstrated that drugs blocking gut microbial TMA production protect against obesity via rewiring circadian rhythms in the gut microbiome, liver, white adipose tissue and skeletal muscle.[33] Furthermore, we also showed that blocking bacterial TMA production elicited unexpected alterations in olfactory perception of diverse odorant stimuli.[46] Therefore, we have followed up here to further interrogate circadian rhythms in the gut microbiome, liver, white adipose tissue (WAT), skeletal muscle, and olfactory bulb in mice lacking the only known host G protein-coupled receptor (GPCR) that senses TMA known as TAAR5.[47,48] In agreement with our previous report showing that *Taar5* mRNA is expressed in a circadian manner in skeletal muscle[33], *LacZ* reporter expression oscillates with highest expression in the dark cycle in muscle (Figure 1A). However, unlike the striking impact that choline TMA lyase inhibitors have on the core circadian clock machinery in skeletal muscle[33], mice lacking the TMA receptor (*Taar5*$^{-/-}$) have unaltered circadian gene expression in muscle (Figure 1A). Instead, *Taar5*$^{-/-}$ mice have alterations in the expression of key circadian genes including *Arntl*, *Clock*, *Nr1d1*, *Cry1*, and *Per2* in the olfactory bulb (Figure 1B). There is also some reorganization of circadian gene expression in the liver (Figure 1C) and gonadal white adipose tissue (Figure 1D), albeit modest. Given the key role that the TMAO pathway plays in suppressing the beiging of white adipose tissue[13], it is important to note that circadian oscillation in genes related to WAT beiging including *Prdm16* and *Ucp1* was altered in *Taar5*$^{-/-}$ mice (Figure 1D). We next examined circadian oscillations in circulating

metabolite, hormone, and cytokine levels in *Taar5*$^{+/+}$ and *Taar5*$^{-/-}$ mice (Figure S1). When we measured substrates for gut microbial TMA production we found that *Taar5*$^{-/-}$ mice had normal oscillations in choline and γ-butyrobetaine, but slightly altered plasma levels of *L*-carnitine particularly in the dark cycle (Figure S1A). *Taar5*$^{-/-}$ mice also had increased levels of TMA at ZT22, when compared to *Taar5*$^{+/+}$ controls (Figure S1A). Interestingly, *Taar5*$^{-/-}$ mice had altered rhythmic levels in host metabolic hormones including insulin, peptide YY (PYY), leptin, ghrelin, and active glucagon-like peptide 1 (GLP-1) (Figure S1B) and modest differences in circulating cytokines including monocyte chemoattractant 1 (MCP-1), interleukin 6 (IL-6), and tumor necrosis factor α (TNFα) (Figure S1B). Collectively, these data demonstrate that *Taar5*$^{-/-}$ mice have altered circadian-related gene expression that is most apparent in the olfactory bulb (Figure 1), and abnormal circadian oscillations in circulating hormones and cytokines (Figure S1).

We next set out to comprehensively analyze the circadian rhythms in behavioral phenotypes in mice lacking the TMA receptor TAAR5. In this line of investigation we took a very broad approach to examine impacts of *Taar5* deficiency on metabolic, cognitive, motor, anxiolytic, social, olfactory and innate behaviors. The main rationale behind this in-depth investigation was to allow for comparison to our recent work showing that pharmacologic blockade of the production of the TAAR5 ligand TMA (using choline TMA lyase inhibitors) produced clear metabolic, innate, and olfactory-related social behavioral phenotypes, but did not dramatically impact aspects of cognition, motor, or anxiolytic behaviors.[33,46]. Also, it is important to note other groups have recently shown that TAAR5 activation with non-TMA ligands or genetic deletion of *Taar5* results in clear olfactory[48-51], anxiolytic[51], cognitive[52], and sensorimotor[53,54] behavioral abnormalities. Here, it was our main goal to identify whether any behavioral phenotypes that were consistently seen in mice lacking bacterial TMA production[33,46] or host TMA sensing by TAAR5 (studied here) are time-of-day dependent indicating circadian inputs. Upon comprehensive behavioral phenotyping, it became very clear that many behavioral phenotypes

in *Taar5*$^{-/-}$ are in most cases gender-specific. For example, only in females we found that startle test response was enhanced, forepaw grip strength was reduced, freezing response during fear conditioning was reduced, and oxygen consumption during cold-induced thermogenesis was increased in *Taar5*$^{-/-}$ mice compared to controls (Figures S2A, S2B, S2F, and S2J). There were also examples of behavioral differences between *Taar5*$^{+/+}$ and *Taar5*$^{-/-}$ mice that were most apparent with both sexes combined (Figures S2C, S2D, and S2E). Also, is important to note that many behavioral phenotypes examined, including tests not shown, were unaltered in *Taar5*$^{-/-}$ mice (Figures S2G, S2H, and S2I). Given the consistent alterations in innate and olfactory-related phenotypes seen in both mice lacking bacterial TMA production[33,46] and mice lacking host TMA sensing by TAAR5 here, we next followed up to perform select innate and olfactory-related behavioral tests in mice at defined circadian time points (Figure 2). To study the circadian presentation of phenotype, we carefully controlled the time window of testing for either the olfactory cookie test or marble burying test, both of which have been shown to be altered in mice lacking bacterial TMA synthesis.[46,55]. When the olfactory cookie test was performed during the mid light cycle (ZT5-ZT7), the latency to find the buried cookie was significantly increased in male *Taar5*$^{-/-}$ mice compared to *Taar5*$^{+/+}$ controls (Figure 2A). However, when the same mice performed the olfactory cookie test at the dark-to-light phase transition (ZT23-ZT1), or at the light-to-dark phase transition (ZT13-ZT15), there was no significant differences between *Taar5*$^{+/+}$ and *Taar5*$^{-/-}$ mice (Figure 2A). When subjected to the marble burying test, only female *Taar5*$^{-/-}$ mice buried significantly more marbles than female wild type controls only at ZT5-ZT7, but this was not apparent at other ZT timepoints Figure 2B). Collectively, these data demonstrate that *Taar5*$^{-/-}$ mice exhibit highly gender-specific alterations in innate and olfactory behaviors, and these behavior phenotypes are only apparent at certain periods within the light cycle (Figures 2, and S2).

Host TAAR5 Regulates the Circadian Rhythmicity of the Gut Microbiome

Bi-directional microbe-host communication is required for homeostatic control of chronobiology in the metaorganism.[56-60] Our data strongly suggest that gut microbe-derived TMA can shape host circadian rhythms in metabolic homeostasis and behavior[33,46], but we also wanted to test whether host TAAR5 may reciprocally regulate circadian rhythms of the gut microbiome[58,59]. When we examined the cecal microbiome in *Taar5*$^{+/+}$ and *Taar5*$^{-/-}$ mice, there were striking alterations that were time of day dependent (Figures 3 and S3). In particular, the oscillatory behavior of several *Lachnospiraceae, Odoribacter*, and *Dubosiella* genera are altered in *Taar5*$^{-/-}$ mice when compared to wild type controls (Figures 3 and S3). Although there were many microbiome alterations, *Taar5*$^{-/-}$ mice showed loss of the normal rhythmicity for *Dubosiella* and *Odoribacter* genera yet gained in amplitude of rhythmicity for *Bacteroides* genera (Figure 3 and S3). It is important to note that previous independent studies have also shown that either blocking bacterial TMA synthesis[33] or FMO3-driven TMA oxidation[29] can also strongly reorganize the gut microbiome in mice. Although more work is needed to fully understand the underlying mechanisms, it is clear that both gut microbe-driven TMA production and host sensing of TMA by TAAR5 (Figures 3 and S3) can strongly impact on circadian oscillations of the gut microbiome.

Mice Genetically Lacking Either Gut Microbial TMA Production or Host-Driven TMA Oxidation Have Altered Circadian Rhythms

To confirm and extend the idea that gut microbe-derived TMA can shape host circadian rhythms we next performed experiments where we genetically deleted either gut microbial TMA synthesis or host-driven TMA oxidation. First, we used gnotobiotic mice engrafted with a defined microbial community with or without genetic deletion of the choline TMA lyase CutC (i.e. *Clostridium sporogenes* wild type versus Δ*cutC*) to understand the ability of gut microbe-derived TMA to alter host circadian rhythms (Figure 4 and S4). Circadian oscillations in plasma TMA and TMAO are only detectable in the group colonized with *C. sporogenes* (WT), but not Δ*cutC C. sporogenes*

(Figure 4A). Other TMAO pathway-related metabolites including choline, *L*-carnitine, γ-butyrobetaine, and betaine exhibit very modest alterations in circadian rhythms (Figure 4A). In a similar manner to *Taar5*$^{-/-}$ mice (Figure 1), mice colonized with Δ*cutC C. sporogenes* show clear alterations in the expression of key circadian genes including *Arntl*, *Clock*, *Nr1d1*, *Cry1*, *Per1*, and *Per2* in the olfactory bulb (Figure 4B). In line with our previous findings that FMO3 suppresses both beige and brown fat-induced cold induced thermogenesis[13], we also found altered expression of key circadian genes (*Arntl*, *Cry1*, *Per2*) and metabolic genes (*Pemt* and *Pdk4*) in subscapular brown adipose tissue (BAT) of Δ*cutC C. sporogenes*-colonized mice (Figure S4A). Furthermore, mice colonized with Δ*cutC C. sporogenes* have altered circadian oscillations in circulating cytokines/chemokines (IL-1β, IL-2, IL-33, IFNγ, and MCP-1), metabolic hormones (leptin and glucagon-like peptide 1), amino acids (tryptophan), and diverse microbe-associated metabolites (indole acetic acid, phenylacetic acid, and phenylacetylglycine) (Figures 4C and S4B). Although gut microbes are the sole source of TMA, circulating levels are also shaped by abundant conversion of TMA to TMAO by the host liver enzyme FMO3[13,29]. To test whether the hepatic conversion of TMA to TMAO by FMO3 may alter circadian rhythms, we necropsied female *Fmo3*$^{+/+}$ and *Fmo3*$^{-/-}$ mice at ZT2 (early light cycle) or ZT14 (early dark cycle). *Fmo3*$^{-/-}$ mice have reduced levels of TMAO at both ZT2 and ZT14, as well as reduced expression of key circadian genes *Arntl* and *Per1* at ZT2 (Figure S4C). Taken together, our data suggest that bacterial production, FMO3-driven metabolism of TMA, as well as sensing of TMA by the host receptor TAAR5, converge to shape circadian rhythms in gene expression, metabolic hormones, gut microbiome composition, and innate behaviors.

Discussion

The metaorganismal TMAO pathway is strongly associated with many human diseases[5-29], which has prompted the rapid development of drugs intended to lower circulating levels of TMAO.[30-37] As the rapid drug discovery advances towards human studies, it will be extremely important to understand the diverse mechanisms by which the primary metabolite TMA and/or the secondary metabolite TMAO promotes disease pathogenesis in the human metaorganism. There is compelling evidence that the end product of the pathway TMAO can promote inflammation, ER stress and platelet activation via activation of NFκB, the NLRP3 inflammasome, PERK, and stimulus-dependent calcium release, respectively.[28,38-41] However, these TMAO-driven mechanisms only partially explain the links to so many diverse human diseases. Here, we provide new evidence that in addition to these TMAO-driven mechanisms, the primary gut microbe TMA can in parallel shape circadian rhythms through the host GPCR TAAR5. The major findings of the current studies are: (1) Mice lacking the TMA receptor TAAR5 have abnormal oscillations in core circadian genes, particularly in the olfactory bulb, (2) Compared to wild type controls, *Taar5*$^{-/-}$ mice have altered circulating levels of cytokines, metabolic hormones, and metabolites at certain times of the day, (3) *Taar5*$^{-/-}$ mice have altered innate and repetitive behaviors that emerge only in a time of day-dependent manner, (4) The normal oscillatory behavior of the cecal microbiome is dysregulated in *Taar5*$^{-/-}$ mice, (5) Genetic deletion of gut microbial choline TMA lyase activity, using defined *cutC*-null microbial communities *in vivo*, results in rewiring of circadian rhythms in gene expression, metabolic hormones, cytokines, and metabolites, and (6) Mice lacking the host liver TMA-to-TMAO converting enzyme FMO3 likewise have altered circadian gene expression in the olfactory bulb. Collectively, our findings suggest that therapeutic strategies designed to limit gut microbial TMA production (i.e. TMA lyase inhibitors), host liver TMA oxidation (i.e. FMO3 inhibitors), or sensing of TMA by the host GPCR TAAR5 (i.e. TAAR5 inhibitors) will need to be carefully evaluated for

pleiotropic effects on circadian rhythms. This body of work also demonstrates that diet-microbe-host interactions can powerfully shape chronobiology, and provides one of the first examples of a microbial metabolite being sensed by a host GPCR to rewire circadian rhythms.

Currently, the only known host receptor that senses gut microbe-produced TMA is the volatile amine receptor TAAR5, which allows for species-specific recognition of the "fishy" odor intrinsic to TMA but not TMAO.[47-49] In general, the trace amine-associated receptor (TAAR) subfamily of GPCRs primarily function as olfactory receptors in vertebrates.[49,50] Ligand-dependent activation of each individual TAAR receptor occurs in a unique sensory neuron population primarily localized to olfactory cilia, and when activated typically elicit TAAR-specific olfactory-related behavior responses[49,50] TMA-dependent activation of TAAR5 was first shown to promote attraction and social interaction between females and male mice in a very species and strain-specific manner.[48] This seminal study by Liberles and colleagues showed that the TMA-TAAR5 olfactory circuit can powerful shape olfactory-driven social interaction, and FMO3-driven conversion of TMA to TMAO suppresses TAAR5 activation.[48] In parallel, we recently performed a comprehensive study to assess cognitive, motor, anxiolytic, social, olfactory and innate behaviors in mice treated with small molecule choline TMA lyase inhibitors to block bacterial TMA production.[46] Much like the olfactory and social phenotypes seen in *Taar5*$^{-/-}$ mice[48], we found that pharmacologic blockade of bacterial TMA production significantly altered olfaction and olfactory-related social behaviors, but did not significantly alter cognitive, motor, anxiolytic behaviors.[46]. It is interesting to note that choline TMA lyase inhibitors altered olfactory perception of several odorant stimuli beyond TMA itself including a cookie, almond, vanilla, corn oil, and coyote urine.[46] This indicates that drugs blocking TMA-TAAR5 signaling could impact olfactory neurogenesis to impact sensing of diverse odorant cues that are well beyond the rotten fish smell intrinsic to TMA. Given that anosmia is a common occurrence in several TMAO-related diseases including CKD[61], obesity, diabetes[62], neurodegenerative diseases[63,64], and COVID-

19[65], it is tempting to speculate that TMA-lowering therapeutics may hold promise to potential restore olfactory perception to diverse stimuli in these disease conditions. However, additional studies are needed to formally test this hypothesis. Given the clear links between the TMA-TAAR5 signaling axis and olfactory-related behaviors in mice[46,48], it will be important to carefully evaluate effects of TMAO-lowering drugs on olfaction in future human studies.

A commonality of many bacterially-derived volatile metabolites is that they have a pungent odor which is sensed by olfactory neurons, and these microbe-host olfactory circuits shape many diverse behavioral and metabolic responses in the human host. For example, strong bacterially-derived odors such as trimethylamine (i.e. smells like rotting fish), hydrogen sulfide (i.e. the rotten egg smell), polyamines including putrescine and cadaverine (i.e. the smell of rotting cadavers/roadkill) can serve as an effective “don't eat me” signal for us to avoid consuming spoiled food. Within the human metaorganism, the gut microbiome and select gut microbe-derived metabolites play an important role in shaping not only food intake but also other aspects of host energy metabolism, insulin sensitivity, immunology, and the circadian clock.[56-60] It is important to note that there is bi-directional communication between gut microbes and the host in maintaining the circadian rhythms in metabolism and immunity within mammalian metaorganisms.[56-60] First, central and peripheral clock machinery in the host clearly shape circadian oscillations in the gut microbiome primarily through innate immune mechanisms.[56,57] At the same time, circadian oscillations intrinsic to the gut microbiome itself can have profound impacts on host physiology and disease.[58-60] Although there is extensive knowledge on how the host circadian clock can impact the oscillatory behavior of the gut microbiome[56,57], much less is known regarding mechanisms by which the gut microbiome can instruct the host circadian clock. Here, we provide one of the first examples of a gut microbe-derived metabolite signaling via a host GPCR to shape circadian rhythms in gene expression, metabolic hormones, gut microbiome composition, and innate behaviors. Using both pharmacologic[33] and genetic

approaches, we have demonstrated that blocking either gut microbial TMA production or sensing by the host TMA receptor TAAR5 results in striking rearrangement of circadian rhythms in the gut microbiome that are linked to metabolic homeostasis and olfactory-related behaviors in mice[33,46]. In further support of the connections between the TMAO pathway and host circadian disruption, a recent paper showed that FMO3 inhibitors blocking host TMA oxidation improved learning and memory deficits driven by chronic sleep loss[66]. Other recent studies in humans also show that TMAO is elevated with sleep deprivation[67], and elevated TMAO levels are associated with an "evening chronotype" that is linked to increased risk of cardiometabolic disease.[68] Collectively, the metaorganismal TMAO pathway plays an important in integrating dietary cues and microbe-host interactions in circadian rhythms. Given TMAO lowering drugs are rapidly advancing towards human studies, it will be of great interest to determine whether these drugs can improve circadian rhythms and potentially synergize with other developmental chronotherapies to improve human health.

Limitations

First, it is critically important to point out that the TMA-TAAR5 signaling axis has evolved to elicit species-specific behavioral responses that differ quite substantially across rodent species and humans.[48,49] When the "stinky" fish odor of TMA is sensed by rat or human TAAR5, the result is typically aversion from consuming what is perceived as rotting food.[48,49] However, select strains of mice have concentration-dependent attraction to low levels of TMA or aversion to high levels of TMA.[48] It has been theorized that this concentration-dependent behavioral response to TMA in mice may have evolved as a kairomone signal that allows mice to sense approaching prey animals.[48,49] Clearly the human TMA-TAAR5 signaling circuit evolved for different reasons in humans, where predator-prey signaling circuits are less prominent. Therefore, additional studies are needed to better understand what diverse roles TMA-driven TAAR5 activation plays in the

circadian rhythms in human metabolism and behavior. The recent discovery of humans with loss-of-function TAAR5 genetic variants[69] may provide a unique population to confirm and extend the findings we report here in mice. Another limitation in our current understanding is that drugs blocking gut microbial TMA production[30-37] or host TMA oxidation[13,15,66] have only been tested in mice. Although these drugs show clear benefit in mice models, the human gut microbiome is quite different than mice and the relative affinity of TMA for TAAR5 is ~ 200-fold less in humans when compared to rodent forms of the receptor.[47-49] Therefore, it is impossible to extrapolate finding in mice to humans. As TMAO lowering drugs move into human trials, there is strong potential that human-specific phenotypes may emerge. A final limitation here is that here we have studied mice globally lacking TAAR5 in all tissues and cell types. Although TAAR5 has primarily been studied in olfactory neurons in the brain, TAAR5 is also expressed in immune cells[70] as well as skeletal and cardiac muscle[33]. Given the expression of TAAR5 outside of the central nervous system, future studies utilizing cell-restricted *Taar5* knockout mice will provide clues into the cell autonomous roles for TMA-TAAR5 signaling. Despite these limitations, a growing body of evidence links TMA-driven TAAR5 activation to circadian regulation of metabolism and olfactory-related behaviors.

Lead contact

Further information and requests for resources and reagents should be directed to and will be fulfilled by the lead contact, J. Mark Brown (brownm5@ccf.org)

Materials availability

All the data and materials that support the findings of this study are available within the article and the *Online Supplement* or available from the lead author upon request.

Data and code availability

All multi-omics datasets are currently being submitted to publicly-available data portals, and accession numbers will be provided upon acceptance of this work.

Code used for cosinor analyses:

1. Sachs, M.C. (2014) cosinor: Tools for estimating and predicting the cosinor model, version 1.1. R package: https://CRAN.R-project.org/package=cosinor.

Any additional information required to reanalyze the data reported in this paper is available from the lead contact (Dr. J. Mark Brown) upon request

Acknowledgements

This work was supported in part by National Institutes of Health grants R01 DK130227 (J.M.B.), P01 HL147823 (J.M.B.), P50 AA024333 (J.M.B.), RF1 NS133812 (J.M.B.), and an American Heart Association Postdoctoral Fellowship 24POST1178494 (S.D.). We are grateful to Dr. Federico Rey (University of Wisconsin – Madison, USA) for providing bacterial strains used in the mouse gnotobiotic studies performed here. We are also grateful to Dr. Stan Hazen for

providing access to mass spectrometer instruments dedicated to targeted metabolomic methods necessary to quantify diverse gut microbe-derived metabolites.

Author Contributions

Conceptualization, K.M. and J.M.B.; methodology, K.M., W.J.M., D.O., A.L.B., T.J., A.C.B., A.J.H., S.D., M.M., N.M., V.V., L.J.O., X.Y., D.M.Y., N.Z., R.H., R.B., P.L., D.L., A.M.H., N.S., M.D., J.A.B., and G.R.S., Z.W; investigation, K.M., W.J.M., D.O., A.L.B., T.J., A.C.B., A.J.H., S.D., M.M., N.M., V.V., L.J.O., X.Y., D.M.Y., N.Z., R.H., R.B., P.L., D.L., N.S., M.D., J.A.B., and Z.W; validation, K.M., W.J.M., A.C.B., A.J.H., S.D., M.M., L.J.O., R.B., P.L., D.L., N.S., M.D., J.A.B., and Z.W; formal analysis, K.M., W.J.M., N.S., T.G., G.R.S., Z.W., J.M.B; writing – original draft, K.M. and J.M.B.; writing – reviewing and editing, K.M., W.J.M., D.O., A.L.B., T.J., A.C.B., A.J.H., S.D., M.M., N.M., V.V., L.J.O., X.Y., D.M.Y., N.Z., R.H., R.B., P.L., D.L., A.M.H., N.S., M.D., J.A.B., G.R.S., and Z.W.; funding acquisition, J.M.B.; supervision, J.M.B.

Declaration of interests

Competing interests: Z.W. reports being named as co-inventor on pending and issued patents held by the Cleveland Clinic relating to cardiovascular diagnostics and therapeutics. Z.W. also reports having received royalty payments for inventions or discoveries related to cardiovascular diagnostics or therapeutics from Cleveland Heart Lab, a fully owned subsidiary of Quest Diagnostics and Procter & Gamble. C.M.T. consults for Abbott Laboratories. J.M.B. reports being named as co-inventor on pending and issued patents held by the Cleveland Clinic relating to choline trimethylamine lyase inhibitors as therapies for cardiometabolic disease including obesity and type 2 diabetes. All other authors: K.M., W.J.M., D.O., A.L.B., T.J., A.C.B., A.H., S.D., M.M.,

N.M., V.V., L.J.O., X.Y., D.M.Y., N.Z., R.H., R.B., P.L., D.L., N.S., T.G., M.D., J.A.B., and G.R.S. have no competing interests.

REFERENCES

1. Aron-Wisnewsky, J., and Clément, K. (2016) The gut microbiome, diet, and links to cardiometabolic and chronic disorders. Nat Rev Nephrol. *12,* 169-181.

2. Nobs, S.P., Zmora, N., Elinav, E. (2020) Nutrition regulates innate immunity in health and disease. Annu Rev Nutr. *40,* 189-219.

3. Arora, T., and Bäckhed, F. (2016) The gut microbiota and metabolic disease: current understanding and future perspectives. J. Intern. Med. *280,* 339-349.

4. Valles-Colomer, M., Menni, C., Berry, S.E., Valdes, A.M., Spector, T.D., and Segata, N. (2023) Cardiometabolic health, diet and the gut microbiome: a meta-omics perspective. Nat Med. *29,* 551-561.

5. Wang, Z., Klipfell, E., Bennett, B.J., Koeth, R., Levison, B.S., Dugar, B., Feldstein, A.E., Britt, E.B., Fu, X., Chung, Y.M., et al. (2011). Gut flora metabolism of phosphatidylcholine promotes cardiovascular disease. Nature *472,* 57-63.

6. Tang, W.H., Wang, Z., Levison, B.S., Koeth, R.A., Britt, E.B., Fu, X., Wu, Y., and Hazen, S.L. (2013) Intestinal microbial metabolism of phoaphatidylcholine and cardiovascular risk. N. Engl. J. Med. *368,* 1575-1584.

7. Koeth, R.A., Wang, Z., Levison, B.S., Buffa, J.A., Org, E., Sheehy, B.T., Britt, E.B., Fu, X., Wu, Y., Li, L., et al. (2013) Intestinal microbiota metabolism of L-carnitine, a nutrient in red meat, promotes atherosclerosis. Nat. Med.*19,* 576-585.

8. Zhu, W., Gregory, J.C., Org, E., Buffa, J.A., Gupta, N., Wang, Z., Li, L., Fu, X., Wu, Y., Mehrabian, M., et al. (2016) Gut microbial metabolite TMAO enhances platelet hyperreactivity and thrombosis risk. Cell *165,* 111-124.

9. Skye, S.M., Zhu, W., Romano, K.A., Guo, C.J., Wang, Z., Jia, X., Kirsop, J., Haag, B., Lang, J.M., DiDonato, J.A., et al. (2018) Microbial transplantation with human gut commensals containing CutC is sufficient to transmit enhanced platelet reactivity and thrombosis potential. Circ. Res. 12*3,* 1164-1176.

10. Bennett, B.J., de Aguiar Vallim, T.Q., Wang, Z., Shih, D.M., Meng, Y., Gregory, J., Allayee, H., Lee, R., Graham, M., Crooke, R., et al. (2013) Trimethylamine-N-oxide, a metabolite associated with atherosclerosis, exhibits complex genetic and dietary regulation. Cell Metab. *17,* 49-60.

11. Koeth, R.A., Levison, B.S., Culley, M.K., Buffa, J.A., Wang, Z., Gregory, J.C., Org, E., Wu, Y., Li, L., Smith, J.D., et al. (2014) gamma-Butyrobetaine is a proatherogenic intermediate in gut microbial metabolism of L-carnitine to TMAO. Cell Metab. *20,* 799-812.

12. Leng, X., Wei, X., Wang, J., Yao, X., Zhang, M., Sun, D., Liang, J., Chi, L., and Cheng, Y. (2025) Impacts of intestinal microbiota metabolite trimethylamine N-oxide on cardiovascular disease: a bibliometric analysis. Front. Microbiol. *15,* 1491731.

13. Schugar, R.C., Shih, D.M., Warrier, M., Helsley, R.N., Burrows, A., Ferguson, D., Brown, A.L., Gromovsky, A.D., Heine, M., Chatterjee, A., et al. (2017) The TMAO-producing enzyme flavin-containing monooxygenase 3 regulates obesity and the beiging of white adipose tissue. Cell Rep. *20,* 279.

14. Dehghan, P., Farhangi, M.A., Nikniaz, L., Nikniaz, Z., and Asghari-Jafarabadi, M. (2020) Gut microbiota-derived metabolite trimethylamine N-oxide (TMAO) potentially increases the risk of obesity in adults: an exploratory systematic review and dose-response meta-analysis. Obes. Rev. *21,* e12993.

15. Miao, J., Ling, A.V., Manthena, P.V., Gearing, M.E., Graham, M.J., Crooke, R.M., Croce, K.J., Esquejo, R.M., Clish, C.B.; Morbid Obesity Study Group; et al. (2015) Flavin-containing monooxygenase 3 as a potential player in diabetes-associated atherosclerosis. Nat. Commun. *6,* 6498.

16. Steinke, I., Ghanei, N., Govindarajulu, M., Yoo, S., Zhong, J., and Amin, R.H. (2020) Drug discovery and development of novel therapeutics for inhibiting TMAO in models of atherosclerosis and diabetes. Front Physiol. *11,* 567899.

17. Tang, W.H., Wang, Z., Kennedy, D.J., Wu, Y., Buffa, J.A., Agatisa-Boyle, B., Li, X.S., Levison, B.S., and Hazen, S.L. (2015) Gut microbiota-dependent trimethylamine N-oxide (TMAO) pathway contributes to both development of renal insufficiency and mortality risk in chronic kidney disease. Circ Res. *116,* 448-455.

18. Zixin, Y., Lulu, C., Xiangchang, Z., Qing, F., Binjie, Z,, Chunyang, L,, Tai, R,, and Dongsheng, O. (2022) TMAO as a potential biomarker and therapeutic target for chronic kidney disease: a review. Front Pharmacol. *13,* 929262.

19. Kumari, S., Goyal, V., Kumaran, S.S., Dwivedi, S.N., Srivastava, A., and Jagannathan, N.R. (2020) Quantitative metabolomics of saliva using proton NMR spectroscopy in patients with Parkinson's disease and healthy controls. Neurol Sci. *41,* 1201-1210.

20. Vogt, N.M., Romano, K.A., Darst, B.F., Engelman, C.D., Johnson, S.C., Carlsson, C.M., Asthana, S., Blennow, K., Zetterberg, H., Bendlin, B.B., and Rey, F.E. (2018) The microbiota-derived metabolite trimethylamine N-oxide is elevated in Alzheimer's disease. Alzheimers Res. Ther. *10,* 124.

21. Xu, R., Wang, Q., and Li, L. (2015) A genome-wide systems analysis reveals strong link between colorectal cancer and trimethylamine N-oxide (TMAO), a gut microbial metabolite of dietary red meat and fat. BMC Genomics *Suppl 7,* S4.

22. Banerjee, R., Wehrle, C.J., Wang, Z., Wilcox, J.D., Uppin, V., Varadharajan, V., Mrdjen, M., Hershberger, C., Reizes, O., Yu, J.S., et al. (2024) Circulating gut microbe-derived metabolites are associated with hepatocellular carcinoma. Biomedicines *12,* 1946.

23. Li, D., Lu, Y., Yuan, S., Cai, X., He, Y., Chen, J., Wu, Q., He, D., Fang, A., Bo, Y., et al. (2022) Gut microbiota-derived metabolite trimethylamine-N-oxide and multiple health outcomes: an umbrella review and updated meta-analysis. Am. J. Clin. Nutr. *116,* 230-243.

24. Heianza, Y., Ma, W., Manson, J.E., Rexrode, K.M., and Qi, L. (2017) Gut microbiota metabolites and risk of major adverse cardiovascular disease events and death: a systematic review and meta-analysis of prospective studies. J Am Heart Assoc. *6,* e004947.

25. Schiattarella, G.G., Sannino, A., Toscano, E., Giugliano, G., Gargiulo, G., Franzone, A., Trimarco, B., Esposito, G., and Perrino C. (2017) Gut microbe-generated metabolite trimethylamine-N-oxide as cardiovascular risk biomarker: a systematic review and dose-response meta-analysis. Eur. Heart J*. 38,* 2948-2956.

26. Jia, J., Dou, P., Gao, M., Kong, X., Li, C., Liu, Z., and Huang, T. (2019) Assessment of causal direction between gut microbiota-dependent metabolites and cardiometabolic health: a bidirectional Medelian Randomization analysis. Diabetes *68,* 1747-1755.

27. Zhou, H., Luo, Y., Zhang, W., Xie, F., Deng, C., Zheng, W., Zhu, S., and Wang, Q. (2023) Causal effect of gut-microbiota-derived metabolite trimethylamine N-oxide on Parkison's disease: A Mendelian randomization study. Eur. J. Neurol. *30,* 3451-3461.

28. Chen, S., Henderson, A., Petriello, M.C., Romano, K.A., Gearing, M., Miao, J., Schell, M., Sandoval-Espinola, W.J., Tao, J., Sha, B., et al. (2019) Trimethylamine N-oxide binds and activates PERK to promote metabolic dysfunction. Cell Metab. *30,* 1141-1151.

29. Zhu, W., Buffa, J.A., Wang, Z., Warrier, M., Schugar, R., Shih, D.M., Gupta, N., Gregory, J.C., Org, E., Fu, X., et al. (2018) Flavin monooxygenase 3, the host hepatic enzyme in the metaorganismal trimethylamine N-oxide-generating pathway, modulates platelet responsiveness and thrombosis risk. J. Thromb. Haemost. *16,* 1857-1872.

30. Wang, Z., Roberts, A.B., Buffa, J.A., Levison, B.S., Zhu, W., Org, E., Gu, X., Huang, Y., Zamanian-Daryoush, M., Culley, M.K, et al. (2015) Non-lethal inhibition of gut microbial trimethylamine production for the treatment of atherosclerosis. Cell *163,* 1585-1595.

31. Roberts, A.B., Gu, X., Buffa, J.A., Hurd, A.G., Wang, Z., Zhu, W., Gupta, N., Skye, S.M., Cody, D.B., Levison, B.S., et al. (2018) Development of a gut microbe-targeted nonlethal therapeutic to inhibit thrombosis potential. Nat. Med. 24, 1407-1417.

32. Organ, C.L., Li, Z., Sharp, T.E. 3rd, Polhemus, D.J., Gupta, N., Goodchild, T.T., Tang, W.H.W., Hazen, S.L., and Lefer, D.J. (2020) Nonlethal inhibition of gut microbial

trimethylamine N-oxide production improves cardiac function and remodeling in a murine model of heart failure. J Am Heart Assoc. *9,* e016223.

33. Schugar, R.C., Gliniak, C.M., Osborn, L.J., Massey, W., Sangwan, N., Horak, A., Banerjee, R., Orabi, D., Helsley, R.N., Brown, A.L., et al. (2022) Gut microbe-targeted choline trimethylamine lyase inhibition improves obesity via rewiring of host circadian rhythms. Elife *11,* e63998.

34. Helsley, R.N., Miyata, T., Kadam, A., Varadharajan, V., Sangwan, N., Huang, E.C., Banerjee, R., Brown, A.L., Fung, K.K., Massey, W.J., et al. (2022) Gut microbial trimethylamine is elevated in alcohol-associated hepatitis and contributes to ethanol-induced liver injury in mice. Elife *11,* e76554.

35. Zhang, W., Miikeda, A., Zuckerman, J., Jia, X., Charugundla, S., Zhou, Z., Kaczor-Urbanowicz, K.E., Magyar, C., Guo, F., Wang, Z., et al. (2021) Inhibition of microbiota-dependent TMAO production attenuates chronic kidney diease in mice. Sci. Rep. *11,* 518..

36. Gupta, N., Buffa, J.A., Roberts, A.B., Sangwan, N., Skye, S.M., Li, L., Ho, K.J., Varga, J., DiDonato, J.A., Tang, W.H.W., and Hazen, S.L.(2020) Targeted inhibition of gut microbial trimethylamine N-oxide production reduces renal tubulointerstitial fibrosis and functional impairment in a murine model of chronic kidney disease. Arterioscler. Thromb. Vasc. Biol. *40,* 1239-1255.

37. Benson, T.W., Conrad, K.A., Li, X.S., Wang, Z., Helsley, R.N., Schugar, R.C,, Coughlin, T.M., Wadding-Lee, C., Fleifil, S., Russell, H.M., et al. (2023) Gut microbiota-derived trimethylamine N-oxide contributes to abdominal aortic aneurysm through inflammatory and apoptotic mechanisms. Circulation *147,* 1079-1096.

38. Seldin, M.M., Meng, Y., Qi, H., Zhu, W., Wang, Z., Hazen, S.L., Lusis, A.J., and Shih, D.M. (2016) Trimethylamine N-oxide promotes vascular inflammation through signaling of mitogen-activated protein kinase and nuclear factor-kB. J. Am. Heart Assoc. *5,* e002767.

39. Sun, X., Jiao, X., Ma, Y., Liu, Y., Zhang, L., He, Y., and Chen, Y. (2016) Trimethylamine N-oxide induces inflammation and endothelial dysfunction in human umbilical vein endothelial cells via activating ROS-TXNIP-NLRP3 inflammasome. Biochem. Biophys. Res. Commun. *481,* 63-70.

40. Chen, M.L., Zhu, X.H., Ran, L., Lang, H.D., Yi, L., and Mi, M.T.(2017) Trimethylamine-N-oxide induces vascular inflammation by activating the NLRP3 inflammasome through the SIRT3-SOD2-mtROS signaling pathway. J. Am. Heart Assoc. *6,* e006347.

41. Zhang, X., Li, Y., Yang, P., Liu, X., Lu, L., Chen, Y., Zhong, X., Li, Z., Liu, H., Ou, C., et al. (2020) Trimethylamine-N-oxide promotes vascular calcification through activation of NLRP3 (Nucleotide-Binding Domain, Leucine-Rich-Containing Family, Pyrin Domain-Containing-3) inflammasome and NF-kB (Nuclear Factor kB) signals. Arterioscler. Thromb. Vasc. Biol. *40,* 751-765.

42. Sulli, G., Manoogian, E.N.C., Taub, P.R., and Panda, S. (2018) Training the circadian clock, clocking the drugs, and drugging the clock to prevent, manage, and treat chronic disease. Trends Pharmacol. Sci. *39,* 812-827.

43. Bolshette, N., Ibrahim, H., Reinke, H., and Asher, G. (2023) Circadian regulation of liver function: from molecular mechanisms to disease pathophysiology. Nat. Rev. Gastroenterol. Hepatol. *20,* 695-707.

44. Zheng, D., Ratiner, K., and Elinav, E. (2020) Circadian influences of diet on the microbiome and immunity. Trends Immunol. *41,* 512-530.

45. Bishehsari, F., Voigt, R.M., and Keshavarzian, A. (2020) Circadian Rhythms and the gut microbiota: from the metabolic syndrome to cancer. Nat. Rev. Endocrinol. *16,* 731-739.

46. Massey, W.J., Kay, K.E., Jaramillo, T.C., Horak, A.J. 3rd, Cao, S., Osborn, L.J., Banerjee, R., Mrdjen, M., Hamoudi, M.K., Silver, D.J.,et al. (2023) Metaorganismal choline metabolism shapes olfactory perception. J. Biol. Chem. *299,* 105299.

47. Wallrabenstein, I., Kuklan, J., Weber, L., Zborala, S., Werner, M., Altmüller, J., Becker, C., Schmidt, A., Hatt, H., Hummel, T., and Gisselmann, G. (2013) Human trace amine-associated receptor TAAR5 can be activated by trimethylamine. PLoS One *8,* e54950.

48. Li, Q., Korzan, W.J., Ferrero, D.M., Chang, R.B., Roy, D.S., Buchi, M., Lemon, J.K., Kaur, A.W., Stowers, L., Fendt, M., and Liberles, S.D. (2013) Synchronous evolution of an odor biosynthesis pathway and behavioral response. Curr. Biol. *23,* 11-20.

49. Liberles, S.D. (2015) Trace amine-associated receptors: ligands, neural circuits, and behaviors. Curr. Opin. Neurobiol. *34* 1-7.

50. Freyberg, Z., and Saavedra, J.M. (2020) Trace amines and trace amine-associated receptors: A new frontier in cell signaling. Cell. Mol. Neurobiol. *40,* 189-190.

51. Espinoza, S., Sukhanov, I., Efimova, E.V., Kozlova, A., Antonova, K.A., Illiano, P., Leo, D., Merkulyeva, N., Kalinina, D., Musienko, P., et al. (2020) Trace amine-associated receptor 5 provides olfactory input into limbic brain areas and modulates emotional behaviors and serotonin transmission. Front. Mol. Neurosci. *13,* 18.

52. Maggi, S., Bon, C., Gustincich, S., Tucci, V., Gainetdinov, R.R., and Espinoza, S. (2022) Improved cognitive performance in trace amine-associated receptor 5 (TAAR5) knock-out mice. Sci. Rep. *12,* 14708.

53. Aleksandrov, A.A., Polyakova, N.V., Vinogradova, E.P., Gainetdinov, R.R., and Knyazeva, V.M. (2019) The TAAR5 agonist alpha-NETA causes dyskinesia in mice. Neurosci Lett. *704,* 208-211.

54. Kalinina, D.S., Ptukha, M.A., Goriainova, A.V., Merkulyeva, N.S., Kozlova, A.A., Murtazina, R.Z., Shemiakova, T.S., Kuvarzin, S.R., Vaganova, A.N., Volnova, A.B., et al. (2021) Role of the trace amine associated receptor 5 (TAAR5) in the sensorimotor functions. Sci. Rep. *11,* 23092.

55. Romano, K.A., Martinez-Del Campo, A., Kasahara, K., Chittim, C.L., Vivas, E.I., Amador-Noguez, D., Balskus, E.P., and Rey, F.E. (2017) Metabolic, epigenetic, and transgenerational effects of gut bacterial choline consumption. Cell Host Microbe. *22,* 279-290.e7.

56. Mukherji, A., Kobiita, A., Ye, T., and Chambon, P. (2013) Homeostasis in intestinal epithelium is orchestrated by the circadian clock and microbiota cues transduced by TLRs. Cell *153,* 812-827.

57. Asher, G., and Sassone-Corsi, P. (2015) Time for food: the intimate interplay between nutrition, metabolism, and the circadian clock. Cell *161,* 84-92.

58. Thaiss, C.A., Zeevi, D., Levy, M., Zilberman-Schapira, G., Suez, J., Tengeler, A.C., Abramson, L., Katz, M.N., Korem, T., Zmora, N., et al. (2014) Transkingdom control of microbiota diurnal oscillations promote metabolic homeostasis. Cell *159,* 514-529.

59. Liang, X., Bushman, F.D., and FitzGerald, G.A. (2015) Rhythmicity of the intestinal microbiota is regulated by gender and the host circadian clock. Proc. Natl. Acad. Sci. U.S.A. *112,* 10479-10484.

60. Choi, H., Rao, M.C., and Chang, E.B. (2021) Gut microbiota as a transducer of dietary cues to regulate host circadian rhythms in metabolism. Nat. Rev. Gastroenterol. Hepatol. *18,* 679-689.

61. Morales Palomares, S., Parozzi, M., Ferrara, G., Andreoli, D., Godino, L., Gazineo, D., Anastasi, G., Sguanci, M., and Mancin, S. (2025) Olfactory dysfunctions and chronic kidney disease: A scoping review. J. Ren. Nutr. *35,* 4-14.

62. Faour, M., Magnan, C., Gurden, H., and Martin, C. (2022) Olfaction in the context of obesity and diabetes: insights from animal models to humans. Neuropharmacology *206,* 108923.

63. Chen, Y.N., and Kostka, J.K. (2024) Beyond anosmia: olfactory dysfunction as a common denominator in neurodegenerative and neurodevelopmental disorders. *Front Neurosci. 18,* 1502779.

64. Papazian, E.J., and Pinto, J.M. (2021) Olfactory loss and aging: connections with health and well-being. Chem. Senses *46,* bjab045.

65. Chang, K., Zaikos, T., Kilner-Pontone, N., and Ho, C.Y. (2024) Mechanisms of COVID-19-associated olfactory dysfunction. Neuropathol. Appl. Neurobiol. *50,* e12960.

66. Zhu, S., Wang, Y., Li, Y., Li, N., Zheng, Y., Li, Q., Guo, H., Sun, J., Zhai, Q., and Zhu, Y. (2024) TMAO is involved in sleep deprivation-induced cognitive dysfunction through regulating astrocytic cholesterol metabolism via SREBP2. Front. Mol. Neurosci. *17,* 1499591.

67. Giskeødegård, G.F., Davies, S.K., Revell, V.L., Keun, H., and Skene, D.J. (2015) Diurnal rhythms in the human urine metabolome during sleep and total sleep deprivation. Sci. Rep. *5,* 14843.

68. Barrea, L., Muscogiuri, G., Pugliese, G., Graziadio, C., Maisto, M., Pivari, F., Falco, A., Tenore, G.C., Colao, A., and Savastano, S. (2021) Association of the chronotype score with circulating trimethylamine N-oxide (TMAO) concentrations. Nutrients. *13,* 1671.

69. Gisladottir, R.S., Ivarsdottir, E.V., Helgason, A., Jonsson, L., Hannesdottir, N.K., Rutsdottir, G., Arnadottir, G.A., Skuladottir, A., Jonsson, B.A., Norddahl, G.L., et al. (2020) Sequence variants in TAAR5 and other loci affect human odor perception and naming. Curr Biol. *30,* 4643-4653.

70. Moiseenko VI, Apryatina VA, Gainetdinov RR, Apryatin SA. (2024) Trace amine-associated receptors' role in immune system function. Biomedicines *12,* 893.

71. Fergusson, G., Ethier, M., Guévremont, M., Chrétien, C., Attané, C., Joly, E., Fioramonti, X., Prentki, M., Poitout, V., and Alquier, T. (2014) Defective insulin secretory response to intravenous glucose in C57Bl/6J compared to C57Bl/6N mice. Mol. Metab. *3,* 848-854.

72. Attané, C., Peyot, M.L., Lussier, R., Zhang, D., Joly, E., Madiraju, S.R., and Prentki, M. (2016) Differential insulin secretion of high-fat diet-fed C57BL/6NN and C57BL/6NJ mice: Implications of mixed genetic background in metabolic studies. PLoS One *11,* e0159165.

73. Massey, W., Osborn, L.J., Banerjee, R., Horak, A., Fung, K.K., Orabi, D., Chan, E.R., Sangwan, N., Wang, Z., and Brown, J.M. (2022) Flavin-containing monooxygenase 3 (FMO3) is critical for dioxin-induced reorganization of the gut microbiome and host insulin sensitivity. Metabolites *12,* 364.

74. Bolyen, E., Rideout, J.R., Dillon, M.R., Bokulich, N.A., Abnet, C.C., Al-Ghalith, G.A., Alexander, H., Alm, E.J., Arumugam, M., Asnicar, F., et al. (2019) Reproducible, interactive, scalable and extensible microbiome data science using QIIME 2. Nat Biotechnol. 37, 852-857.

75. Callahan, B.J., McMurdie, P.J., Rosen, M.J., Han, A.W., Johnson, A.J., and Holmes, S.P. (2016) DADA2: high-resolution sample inference from Illumina amplicon data. Nat. Methods 13, 581–583.

76. McMurdie, P.J., and Holmes, S. phyloseq: an R package for reproducible interactive analysis and graphics of microbiome census data. PLoS OneApr 8, e61217.

77. Benjamini, Y., and Hochberg, Y, (1995). Controlling the false discovery rate: A practical and powerful approach to multiple testing, Journal of the Royal Statistical Society, Series B: Methodological *57,* 289–300.

78. Cornelissen, G. (2014) Cosinor-based rhythmometry. Theorectial Biology & Medical Modelling. *11,* 16.

79. Fernandes, A.D., Reid, J.N., Macklaim, J.M., McMurrough, T.A., Edgell, D.R., and Gloor, G.B. (2014) Unifying the analysis of high-throughput sequencing datasets: characterizing RNA-seq, 16S rRNA gene sequencing and selective growth experiments by compositional data analysis. Microbiome *2,* 15.

80. Nelson, W., Tong, Y.L., Lee, J.K., and Halberg, F. (1979) Methods for cosinor-rhythmometry. Chronobiologia *6,* 305-323.

81. Bingham, C., Arbogast, B., Guillaume, G.C., Lee, J.K., and Halberg, F. (1982) Inferential statistical methods for estimating and comparing cosinor parameters. Chronobiologia *9,* 397-439.

HIGHLIGHTS

- Mice lacking the host TMA receptor (*Taar5*$^{-/-)}$ have altered circadian rhythms.
- *Taar5*$^{-/-}$ mice have altered innate behaviors in a time of day dependent manner.
- The normal circadian oscillations in the gut microbiome are dysregulated in *Taar5*$^{-/-}$ mice.
- Genetic deletion of bacterial TMA production or host TMA oxidation shapes circadian rhythms.

eTOC BLURB

The metaorganismal TMAO pathway is strongly associated with cardiometabolic disease, yet mechanisms underlying this are incompletely understood. Mahen *et al.* now show that microbial TMA production and host TMA sensing via TAAR5 broadly alter host circadian rhythms in gene expression, metabolic hormones, gut microbiome, and innate behaviors.

ABBREVIATIONS USED

Arntl, basic helix-loop-helix ARNT like 1 or Bmal1; BAT, brown adipose tissue; CKD, chronic kidney disease; *Cry1*, cryptochrome 1; *Cry2*, cryptochrome 2; CVD, cardiovascular disease; EIF2AK3, eukaryotic translation initiation factor 2-alpha kinase 3; ER, endoplasmic reticulum; FMO3, flavin containing monooxygenase 3; GPCR, G protein-coupled receptor; IFNγ, interferon gamma; IL; interleukin; MCP-1, monocyte chemoattractant protein-1; NFκB, nuclear factor κB; NLRP3, nucleotide-binding domain, leucine-rich-containing family, pyrin domain-containing-3; *Nr1d1*, nuclear receptor subfamily 1 group D member 1 or REV-ERBalpha; Pemt, phosphatidylethanolamine *N*-methyltransferase; PERK, eukaryotic translation initiation factor 2-alpha kinase 3; *Per1*, period 1; *Per2*, period 2; *Taar5*, trace amine associated receptor 5; TMA, trimethylamine; TMAO, trimethylamine oxide; WAT, white adipose tissue; ZT, zeitgeber time.

STAR★Methods

Key resources table

REAGENT or RESOURCE	SOURCE	IDENTIFIER
Bacterial and virus strains		
Bacteroides thetaiotaomicron	ATCC	VPI-5482
Bacteroides caccae	ATCC	ATCC 43185
Bacteroides ovatus	ATCC	ATCC 8483
Collinsella aerofaciens	ATCC	ATCC 25986
Eubacterium rectale	ATCC	ATCC 33656
Clostridium sporogenes	ATCC	ATCC 15579
Clostridium sporogenes ΔcutC	Dr. Michael Fischbach at Stanford University	N/A
Chemicals, peptides, and recombinant proteins		
Choline chloride	Sigma	#C7017
Choline chloride (trimethyl-D_9, 98%)	Cambridge Isotope Laboratories, Inc.	#DLM-549-MPT-PK
Betaine	Sigma	#61962
N-(Carboxymethyl)-N,N,N-trimethyl-d9-ammonium Chloride	C/D/N Isotopes Inc.	#D-3352
L-Carnitine hydrochloride	Sigma	#94954
L-Carnitine-d3 HCl (N-methyl-d3)	C/D/N Isotopes Inc.	#D-5069
(3-Carboxypropyl)trimethylammonium chloride (butyrobetaine)	Sigma	#403245
Butyrobetaine-d9	Wang, Z. *et al.*[30]	NA
5-hydroxyindole-3-acetic acid	Sigma	#H8876
5-Hydroxyindole-3-Acetic-2,2-D2 Acid	CDN Isotopes	#D-1547
hippuric acid	Sigma	#8206490100
N-Benzoyl-d5-glycine	CDN Isotopes	#D-5588
4-OH-Hippuric acid	Santa Cruz Biotechnology	#SC-277427
3-hydroxyhippuric acid	TRC	#H943125
2-Hydroxyhippuric Acid	Carbosynth	#FH240191601
Indole-3-Propionic Acid	Alfa Aesar	#L04877
Indole-3-Propionic-2,2-D2 Acid	CDN Isotopes	#D-7686
Methylindole-3-Acetate	Sigma	#I9770
DL-Indole-3-Lactic Acid	Chem-Impex	#21729
Phenylacetic acid	Aldrich	#P16621
Phenylacetic Acid-1,2-13C2	Chem Cruz	#SC-236371
DL-p-Hydrophenyllactic Acid	Aldrich	#H3253
Indoxyl-Glucuronide	Abcam	#Ab146380
L-Tryptophan-2',4',5',6',7'-d5 (indole-d5)	CDN Isotopes	#D-1522
serotonin	Sigma	#H-9523
Tryptamine	Aldrich	#193747
Tryptamine-α,α,β,β-D4 HCl	CDN Isotopes	#D-1546
3-Indoleacetic Acid	Aldrich	#I3750
Indole-3-Acetic-2,2-D2 Acid	CDN Isotopes	#D-1709
Sodium phenyl sulfate	Enamine	#EN300-1704008
TMAO	Sigma	#317594
Trimethylamine *N*-oxide (D_9, 98%)	Cambridge Isotope Laboratories, Inc.	#DLM-4779-1

Phenylacetyl-L-Glutamine	Chem-Impex	#16414
N-alpha-(phenyl-d5-acetyl)-L-glutamine	CDN Isotopes	#D-6900
Potassium p-tolyl sulfate P-cresol sulfate K-salt)	TCI	#P2091
p-Cresol sulfate, potassium salt (D_7, 98%)	Cambridge Isotope Laboratories, Inc.	#DLM-9786
3-Indoxyl Sulfate Potassium Salt	Chem-Impex	#21710
3-Indoxyl Sulfate-d4 Potassium Salt	TRC	#I655102
Phenylacetylglycine	Bachem	#4016439
trans-3-Indoleacrylic acid	Aldrich	#I3807
4-Ethylphenyl sulfate Potassium salt	TRC	#E925865
Trimethylamine hydrochloride	Sigma	#41284
Trimethylamine:DCl (D_{10}, 98%)	Cambridge Isotope Laboratories, Inc.	#DLM-1817-5
Critical commercial assays		
Monarch Total RNA Miniprep Kit	New England BioLabs	#T2010S
V-Plex Cytokine Panel 1 Mouse Kit	Mesoscale Discovery	#K15245D
V-Plex Pro-Inflammatory Panel 1 Mouse Kit	Mesoscale Discovery	#K15048D
U-Plex Metabolic Combo Mouse Kit	Mesoscale Discovery	#K15297K
Ultra Sensitive Mouse Insulin ELISA	Crystal Chem Inc.	#90080
DNeasy PowerSoil Pro Kit	Qiagen	#47014
Experimental models: Organisms/strains		
Germ/free C57BL/6NTac	Taconic	Stock #: B6-GF-F
C57BL/6J	Jackson	#00664
C57BL/6J *Taar5*$^{-/-}$	This paper	NA
C57BL/6J *Fmo3*$^{-/-}$	Massey *et al.*[73]	NA
Oligonucleotides		
LacZ Forward: CCAACGTGACCTATCCCATTAC	Sigma	NA
LacZ Reverse: ATCTTCCTGAGGCCGATACT	Sigma	NA
Arntl1 Forward: CCAAGAAAGTATGGACACAGACAAA	Sigma	NA
Arntl1 Reverse: GCATTCTTGATCCTTCCTTGGT	Sigma	NA
Nr1d1 Forward: ATGCCAATCATGCATCAGGT	Sigma	NA
Nr1d1 Reverse: CCCATTGCTGTTAGGTTGGT	Sigma	NA
Per1 Forward: TGTCCTGGTTTCGAAGTGTG	Sigma	NA
Per1 Reverse: TGTGTCAAGCAGGTTCAGG	Sigma	NA
Per2 Forward: GCTGACGCACACAAAGAACT	Sigma	NA
Per2 Reverse: TAGCCTTCACCTGCTTCACG	Sigma	NA
Clock Forward: AGGCACAGACATTATCGG	Sigma	NA
Clock Reverse: ACCGTCTCATCAAGGGAC	Sigma	NA
Cry1 Forward: TACTGGGAAACGCTGAACCC	Sigma	NA
Cry1 Reverse: ACCCCAAGCTTGTTGCCTAA	Sigma	NA
Cry2 Forward: GCTGGAAGCAGCCGAGGAACC	Sigma	NA
Cry2 Reverse: GGGCTTTGCTCACGGAGCGA	Sigma	NA
Prdm16 Forward: CAGCACGGTGAAGCCATTC	Sigma	NA
Prdm16 Reverse: GCGTGCATCCGCTTGTG	Sigma	NA
Ucp1 Forward: ACTGCCACACCTCCAGTCATT	Sigma	NA
Ucp1 Reverse: CTTTGCCTCACTCAGGATTGG	Sigma	NA
Pemt Forward: TGTGCTGTCCAGCTTCTATG	Sigma	NA
Pemt Reverse: GAAGGGAAATGTGGTCACTCT	Sigma	NA
Pdk4 Forward: GTGCTCTCTGGTCCTCTGTG	Sigma	NA
Pdk4 Reverse: AGTCCAACGGACAAAACGGA	Sigma	NA
Fmo3 Forward: CCCACATGCTTTGAGAGGAG	Sigma	NA

Fmo3 Reverse: GGAAGAGTTGGTGAAGACCG	Sigma	NA
CycloA Forward: GCGGCAGGTCCATCTACG	Sigma	NA
CycloA Reverse: GCCATCCAGCCATTCAGTC	Sigma	NA
Gapdh Forward: CCTCGTCCCGTAGACAAAATG	Sigma	NA
Gapdh Reverse: TGAAGGGGTCGTTGATGGC	Sigma	NA
Software and algorithms		
GraphPad Prism	https://www.graphpad.com/	Version 10.4.1
DADA2	https://benjjneb.github.io/dada2/	Version 3.16
metagenomeSeq	https://github.com/HCBravoLab/metagenomeSeq	Version: Release (3.20)
DAtest	https://github.com/Russel88/DAtest	Version 2.8.0.
ggplot2	https://cran.r-project.org/web/packages/ggplot2/index.html	Version 3.5.1
cosinor	https://cran.r-project.org/web/packages/cosinor/index.html	Version 1.2.3
cosinor2	https://cran.r-project.org/web/packages/cosinor2/index.html	Version 0.2.1
EthoVision XT15 (video tracking software)	Noldus	NA
Other		
qScript	QuantaBio	#95048-100
Fast SYBR Green Master Mix	Applied Biosystems	#4385612
Nutter Butter Cookies	Nabisco	NA
Marbles	Moon Marble Company	NA
SR-LAB-Startle Response System	San Diego Instruments	#2325-0400
Elevated Plus Maze	Nationwide Plastics	NA
Y Maze	Nationwide Plastics	NA
Forepaw Grip Strength Meter	Columbus Instruments	#1027SM
Rotamex-5	Columbus Instruments	#0254–8000
Fear Conditioning Chambers	Med Associates	#VFC-008
Hot Plate	Ugo Basile	#35300
OxyMax Clams Home Cage System	Columbus Instruments	NA

EXPERIMENTAL PROCEDURES

Animal Studies (Mice)

Taar5$^{-/-}$ mice [Taar5$^{tm1.1(KOMP)Vlcg}$] used here were created from ES cell clone 10675A-A8 and originated on the C57BL/6N background by Regeneron Pharmaceuticals, Inc. The successfully

targeted ES cells were then used to create live mice by the KOMP Repository and the Mouse Biology Program at the University of California Davis. It is important to note that this KO/reporter mouse line has the removal of the neomycin selection cassette and critical exon(s) leaving behind the inserted *lacZ* reporter sequence knocked into the *Taar5* locus. Given the well appreciated differences in metabolic homeostasis between C57BL/6N and C57BL/6J substrains[71,72], we backcrossed this line > 10 generations into the C57BL/6J congenic strain and backcrossing was confirmed by mouse genome SNP scanning at the Jackson Laboratory (Bar Harbor, ME). Heterozygous mice on a pure C57BL/6J background were bred to generate littermate *Taar5*$^{+/+}$ and *Taar5*$^{-/-}$ mice. Global *Fmo3*$^{-/-}$ mice on a pure C57BL/6J background have been previously described.[73] All mice were fed standardized control chow diet with defined sufficient level of dietary choline (Envigo diet TD:130104) that was twice irradiated for sterilization. For studies of circadian rhythms, 9-week-old C57Bl6/J male mice were adapted for 2 weeks with a strict 12:12 light:dark cycle. After 7 days, plasma and tissue were collected every 4 hours over a 24-hour period. All dark cycle necropsies were performed under red light conditions to avoid light-driven circadian cues. For the CutC mutant studies shown in main Figure 4, 7-8 week-old germ-free B6/N mice were purchased from Taconic and placed on a sterile chow. Two weeks later, the mice were given an oral gavage of our 6 member community that included *B. caccae, B. ovatus, B. theta, C. aerofaciens, E. rectale, and either wildtype or mutant C. sporogenes* suspended in sterile PBS + 20% glycerol as previously described.[55] Gnotobiotic colonized mice were maintained using the Allentown Sentry SPP Cage System (Allentown, NJ) on a 14 hr:10 hr light:dark cycle. Mice were transferred to a room equipped with 12:12 light-dark cycling while still housed on Allentown Transport Carts. After one week of acclimation, plasma and tissue collection were performed every 4 hours over a 24-hour period. All dark cycle necropsies were performed under red light conditions. For all studies plasma was collected by cardiac puncture, and liver, GWAT, BAT and olfactory bulb were collected, flash-

frozen, and stored at –80°C until the time of analysis. All mice were maintained in an Association for the Assessment and Accreditation of Laboratory Animal Care, International-approved animal facility, and all experimental protocols were approved by the Institutional Animal Care and use Committee of the Cleveland Clinic (Approved IACUC protocol numbers 00001941, 00002609, and 0002866).

RNA and Realtime PCR Methods

RNA isolation and quantitative polymerase chain reaction (qPCR) was conducted using methods previously described with minor modifications. [13,33,46] To extract RNA, the Monarch Total RNA MiniPrep Kit (New England BioLabs, Inc.) was employed, and 325 ng of cDNA was utilized for Realtime PCR on a 384-well plate, using Applied Biosystem's Power SYBR Green PC mix in Roche LightCycler 480 I1. The levels of induced mRNAs were standardized by the ΔΔCT method and were normalized to cyclophilin A. The specificity of the primers was verified by analyzing the melting curves of the PCR products. Primer information is available in the Star Methods table.

Quantification of Plasma Metabolites Using Liquid Chromatography Tandem Mass Spectrometry (LC-MS/MS)

Stable isotope dilution high-performance LC-MS/MS was used for quantification of levels of TMAO, TMA, choline, carnitine, and γ-butyrobetaine and all other reported circulating plasma metabolites as previously described performed on a Shimadzu 8050 triple quadrupole mass spectrometer.[13,33,46] A subset of samples were also analyzed on a Thermo Vanquish liquid chromatograph coupled with a Thermo TSQ Quantiva mass spectrometer. 0.2% of formic acid in water (LC-MS grade) was used as mobile phase A and 0.2% formic acid in acetonitrile was used as mobile phase B. The separation was conducted using the following gradient: 0 min, 5% B; 0-2 min, 5% B; 2-8 min, 5%-100%B; 8-16 mins, 100%B; 16-16.5 mins, 5%B; 16.5-25 mins,

5%B. The flow rate was set at 0.2 ml/min. Samples were injected at 2 µl onto a Phenomenex Gemini C18 analytical column (2.0×150 mm, 3 µm). Column temperature was set at 25°C. The acquired data were processed by Thermo Xcalibur 4.3 software to calculate the concentrations. Both methods used multiple reaction monitoring of precursor and characteristic products as we have previously described. [13,33,46]

Plasma Hormone and Cytokine Quantification

Plasma hormones and cytokine levels were quantified using U-PLEX (product # K15297K) and V-PLEX (K15297K) assays per the manufacturer's instructions (Meso Scale Diagnostics, Rockville, Maryland, USA).

Olfactory Cookie Test

To broadly understand olfactory perception, we performed the olfactory cookie test using methods previously described.[46] Briefly, one day prior to testing, food was removed from the home cage. The following day, a clean cage was filled with ~1.5 inches of clean bedding and a small portion of peanut butter cookie (Nutter Butter, Nabisco®) was placed randomly ~1 cm under the bedding. A test mouse was placed into the cage and given 10 minutes to find the hidden cookie. Latency to find the cookie was recorded.

Marble Burying Test

To test for innate/repetitive behavioral alterations, mice underwent a marble burying test. A clean mouse cage was filled with 2.5-3 inches of bedding. 20 black marbles were placed evenly in 5 rows of 4 across the bedding. A test mouse was placed into the cage and was allowed to bury marbles for 30 minutes. After 30 minutes the number of marbles buried was counted. A marble was defined as buried when < 25% of the marble was visible.

Pre-Pulse Inhibition and Startle Test

Mice underwent a PPI and startle threshold test using methods previously described.[46] On day 1 PPI was measured and on Day 2 startle threshold was measured. Mice were placed inside holding cylinders that sit atop of a piezoelectric accelerometer that detects and transduces animal movement (SR-LAB Startle Response System; SD Instruments; San Diego, CA). Acoustic stimuli were delivered by high-frequency speakers mounted 33 cm above the cylinders. Mouse movements were digitized and stored using computer software supplied by San Diego Instruments. From the onset of startle stimuli, 65 1-ms readings were recorded, and the amplitude of the startle responses was obtained in arbitrary units. Chambers were calibrated before testing, and sound levels were monitored using a sound meter (Tandy). For prepulse inhibition (PPI), mice were subjected to five trial types in a 22 min session: pulse alone (40 ms, 120 dB, white noise pulse), three different prepulse/pulse trials (20 ms prepulse of 4, 8, or 16 dB above background noise level of 70 dB preceded the 120-dB pulse by 100 ms onset–onset interval), and no stimulus. All trials were presented pseudo randomly with an average of 15 s (7–23 s) between the 62 trials. Testing began with a 5 min acclimation to the cylinders, followed by four blocks of test trials. The first and last blocks consisted of six pulse-alone trials. Blocks 2 and 3 each contained six pulse-alone trials, five of each level of prepulse/pulse trials, and five no-stimulus trials. Data were analyzed for baseline startle amplitude (initial pulse-alone trials) and PPI (percentage decrease in startle amplitude for prepulse/pulse trials compared with pulse-alone trials). The next day the startle reactivity test was conducted in a similar manner except eight presentations of six trial types were given in pseudorandom order: no stimulus, 80, 90-, 100-, 110-, or 120-dB pulses. Mean startle amplitudes for each condition were calculated.

Forepaw Grip Strength Test

Grip strength was measured using a digital grip meter (Chatillon Guage with Mesh bar; Columbus Instruments, Columbus, OH) in which a mouse was suspended by its tail and allowed to grab onto a stainless-steel grid bar that is attached to a force transducer. The mouse was gently pulled away from the meter in a horizontal plane. The force applied to the bar immediately before the mouse released its grip was recorded in grams force by the digital sensor. Mice completed 10 trials with an intertrial interval of a least 30 seconds. The mouse's reported grip strength was the average of all 10 trials.

Hotplate Sensitivity Test

For the hotplate sensitivity test, each mouse received a single trial that lasted a maximum of 30 seconds, and the behavioral response was scored live. To assess sensitivity to hot stimuli, a hot plate (Ugo Basile, Italy) was warmed to 52°C and a mouse was placed on the plate and a tall plexiglass cylinder was placed around the mouse to prevent the animal from leaving. A foot pedal was pressed to start the timer on the hotplate. As soon as the mouse showed a response to the stimuli such as jumping or licking their paws, the foot pedal was pressed again to stop the timer and the mouse was removed from the plate. Latency to respond was recorded.

Rotarod

This was a 2-day task in which mice were placed onto a nonrotating rod (3 cm in diameter) that had ridges for a mouse to grip and was divided into 4 sections that allowed 4 mice to be tested at the same time (Rotamex-5; Columbus Instruments; Columbus, OH). Each mouse was subjected to 4 trials per day with an inter-trial interval of at least 30 minutes to prevent its performance from being impaired by fatigue. For each trial, a mouse was placed onto the rod and allowed to balance itself. When mice were balanced on the rod, the rod started rotating and accelerated from 4 to 40 rpm over a 5-minute period. Latency to stay onto the rod was assessed

with the use of an infrared beam just above the rod and was broken once the mouse fell off the rod. Each mouse was subjected to a total of 8 trials over a 2-day period (4 trial/day). Latency to fall (seconds) was recorded.

Social Behavior

Social interaction with a juvenile was performed in a novel empty home cage under dim white light as described previously.[46] Briefly, following a 15-min habituation, a test mouse was placed in a novel empty cage with a juvenile stimulus mouse (BALB/cJ juvenile mouse; 3 weeks of age; Stock #000651 Jackson Labs) and was allowed to directly interact for 2 min. Interaction was scored by observing the duration and number of times the test mouse-initiated contact with or sniffed the juvenile mouse. Contact was considered as any part of the body touching the other mouse. Three days later the same test mouse and juvenile mouse were paired again in a novel clean cage for 2 min and scored in the same manner.

Fear Conditioning

Fear conditioning (FC) consisted of a training period and a testing period. For the training period, mice were placed in the fear conditioning boxes (Med Associates; Fairfax VT), with a gridded floor, an inside white light and NIR light, and a fixed NIR camera for video recording. Mice were placed inside the chamber for 2 minutes, and then a 30 second, 90 dB acoustic conditioned stimulus (CS; white noise) co- terminated with a 2 second 0.6 mA foot shock (US). Mice received a total of 3 US-CS pairing, with each pairing separated by 1 minute. The mouse remained in the chamber for 30 seconds after the pairings before returning to its home cage. The testing period occurred 24-hrs after the training period ended. The mouse's freezing behavior (motionless except for respirations) was monitored during testing to access memory. Contextual FC consisted of placing the mouse back into the same chamber as was done with training for 5

minutes and measuring freezing behavior. No shock or sound was presented to the mouse, just the context of the chamber. Later that day, mice were brought back to test for cue fear conditioning. Prior to cue FC testing, the inside of the FC chamber was modified using white plastic sheets, interior lighting, and vanilla extract on a paper towel placed in the bedding chamber to make the chamber look and smell differently than the training period. Mice were placed into this modified chamber and allowed to habituate for 3 minutes. Following 3 minutes the same white noise tone used in training was presented to the mouse for 3 minutes. During the tone presentation mouse freezing behavior was recorded. Total percent freezing for context and cue FC was recorded.

Elevated Plus Maze

The elevated plus maze task was conducted essentially as described previously.[64] Mice were placed in the center of a black, plexiglass elevated plus maze (each arm 33 cm long and 5 cm wide with 25 cm high walls on closed arms) in a dimly lit room for 5 minutes. Automated video tracking software from Noldus Ethovision XT13 (Leesburg VA) was used to track time spent in the open and closed arms, number of open and closed arm entries, and number of explorations of the open arm (defined as placing head and two limbs into open arm without full entry).

Y-Maze

Spontaneous alteration in Y-Maze was assessed as previously described.[64] Briefly, a mouse was placed into one arm of the Y-maze facing the center (14”). Video-tracking was used to record the spontaneous behavior of each mouse for 10 min. Zone (i.e. arm) alteration was later analyzed using Noldus EthoVision XT14, to determine when a mouse entered 3 consecutive different arms of the maze. Spontaneous alteration % was calculated as follows: Alteration % = #spontaneous alterations/ total number of arm entries -2 x 100.

Indirect Calorimetry and Metabolic Cage Measurements During Cold Challenge

Cold-induced metabolic responses were quantified using the Oxymax CLAMS system (Columbus Instruments) as previously described.[13] Briefly, weight matched *Taar5*$^{-/-}$ and *Taar5*$^{+/+}$ mice were acclimated to metabolic cages for 48 hours. Thereafter, physical activity, oxygen consumption (VO_2), carbon dioxide production (VCO_2), and respiratory exchange ratio (RER) were continually monitored for 24 hours at thermoneutrality (30°C), 24 hours at room temperature 22°C, and 24 hours in the cold (4°C). Data represent the last 6 a.m. to 6 a.m. period after adequate acclimation.

16S rRNA gene amplicon sequencing and bioinformatics

16S rRNA gene amplicon sequencing and bioinformatics analysis were performed using our published methods.[33] Briefly, raw 16S amplicon sequence and metadata, were *demultiplexed using split_libraries_fastq.*py script implemented *in QIIME2.*[74] Demultiplexed fastq file was split into sample-specific fastq files using split_sequence_file_on_sample_ids.py script from QIIME2. Individual fastq files without non-biological nucleotides were processed using Divisive Amplicon Denoising Algorithm (DADA) pipeline.[75] The output of the dada2 pipeline [feature table of amplicon sequence variants (an ASV table)] was processed for alpha and beta diversity analysis using *phyloseq*[76], and microbiomeSeq (http://www.github.com/umerijaz/microbiomeSeq) packages in R. We analyzed variance (ANOVA) among sample categories while measuring the of α-diversity measures using plot_anova_diversity function in *microbiomeSeq* package. Permutational multivariate analysis of variance (PERMANOVA) with 999 permutations was performed on all principal coordinates obtained during CCA with the *ordination* function of the *microbiomeSeq* package. Pairwise correlation was performed between the microbiome

(genera) and metabolomics (metabolites) data was performed using the microbiomeSeq package.

16S Statistical Analysis

Differential abundance analysis was performed using the random-forest algorithm, implemented in the DAtest package (https://github.com/Russel88/DAtest/wiki/usage#typical-workflow). Briefly, differentially abundant methods were compared with False Discovery Rate (FDR), Area Under the (Receiver Operator) Curve (AUC), Empirical power (Power), and False Positive Rate (FPR). Based on the DAtest's benchmarking, we selected lefseq and anova as the methods of choice to perform differential abundance analysis. We assessed the statistical significance ($P < 0.05$) throughout, and whenever necessary, we adjusted *P*-values for multiple comparisons according to the Benjamini and Hochberg method to control False Discovery Rate.[77] Linear regression (parametric test), and Wilcoxon (Non-parametric) test were performed on genera and ASVs abundances against metadata variables using their base functions in R (version 4.1.2; R Core Team, 2021).

Data Analyses for Circadian Rhythmicity (Cosinor Analyses)

A single cosinor analysis was performed as previously described.[78,79] Briefly, a cosinor analysis was performed on each sample using the equation for cosinor fit as follows:

$$Y(t)=M+A\cos(2\theta/\tau+\phi)$$

where M is the MESOR (midline statistic of rhythm, a rhythm adjusted mean), A is the amplitude (a measure of half the extent of the variation within the cycle), Φ is the acrophase (a measure of the time of overall highest value), and τ is the period. The fit of the model was determined by the

residuals of the fitted wave. After a single cosinor fit for all samples, linearized parameters were then averaged across all samples allowing for calculation of delineralized parameters for the population mean. A 24 hr period was used for all analysis. Comparison of population MESOR, amplitude, and acrophase was performed as previously described.[33] Comparisons are based on F-ratios with degrees of freedom representing the number of populations and total number of subjects. All analyses were done in R v.4.0.2 using the cosinor and cosinor2 packages.[79-81]

Standard Statistical Analyses

Data are expressed as the mean ± standard error of the mean (SEM). All data were analyzed using either one-way or two-way analysis of variance followed by Student's t tests for post hoc analysis. Differences were considered significant at $p < 0.05$. All analyses were performed using GraphPad Prism software (version 10.2.2; GraphPad Software, Inc).

Figure Legends

Figure 1. The Host Trimethylamine Receptor TAAR5 Shapes Tissue-Specific Circadian Oscillations. Male chow-fed wild type (*Taar5*$^{+/+}$) or mice lacking the TMA receptor (*Taar5*$^{-/-}$) were necropsied at 4-hour intervals to collect tissues including skeletal muscle **(A)**, olfactory bulb **(B)**, liver **(C)**, or gonadal white adipose tissue **(D)**. The relative gene expression for circadian and metabolism related genes was quantified by qPCR. Data shown represent the means -/+ S.D. for n= 3-6 individual mice per group. Group differences were determined using cosinor analyses *p*-values are provided where there were statistically significant differences between *Taar5*$^{+/+}$ and *Taar5*$^{-/-}$ mice. The complete cosinor statistical analysis for circadian data can be found in Table S1. * = Significant differences between *Taar5*$^{+/+}$ and *Taar5*$^{-/-}$ mice by student's t-tests within each ZT time point ($p<0.05$).

Figure 1 – Figure Supplement 1. The Host Trimethylamine Receptor TAAR5 Shapes Circadian Oscillations in Circulating Hormones and Cytokines. Male chow-fed wild type mice (*Taar5*$^{+/+}$) or mice lacking the TMA receptor (*Taar5*$^{-/-}$) were necropsied at 4-hour intervals to collect plasma. **(A)** Plasma levels of metabolites in the metaorganismal trimethylamine N-oxide (TMAO) pathway were quantified using liquid chromatography tandem mass spectrometry (LC-MS/MS). **(B)** Plasma hormones and cytokine levels were quantified as described in the material and methods. Data shown represent the means -/+ S.D. for n= 3-6 individual mice per group. Group differences were determined using cosinor analyses *p*-values are provided where there were statistically significant differences between *Taar5*$^{+/+}$ and *Taar5*$^{-/-}$ mice. The complete cosinor statistical analysis for circadian data can be found in Table S1. * = Significant differences between *Taar5*$^{+/+}$ and *Taar5*$^{-/-}$ mice by student's t-tests within each ZT time point ($p<0.05$).

Figure 2. Mice Lacking the Host TMA Receptor TAAR5 Have Altered Olfactory and Repetitive Behaviors Only at Specific Circadian Timepoints. Male or female wild type mice (*Taar5*$^{+/+}$) or mice lacking the TMA receptor (*Taar5*$^{-/-}$) were subjected to the olfactory cookie test **(A)** or the marble burying test **(B)**. To examine circadian alterations in behavior, these tests were done in either the dark-light phase transition (ZT23-ZT1), mid light cycle (ZT5-ZT7), or early dark cycle (ZT13-ZT15). Data represent the mean -/+ S.E.M., and statistically significant difference between *Taar5*$^{+/+}$ and *Taar5*$^{-/-}$ mice are denoted by * = $p<0.05$ and ** = $p<0.01$.

Figure 2 – Figure Supplement 1. Mice Lacking the Host TMA Receptor TAAR5 Have Altered Behaviors. Male or female wild type mice (*Taar5*$^{+/+}$) or mice lacking the TMA receptor (*Taar5*$^{-/-}$) were subjected to a battery of behavioral test including: **(A)** startle test, **(B)** forepaw grip strength test, **(C)** hotplate sensitivity test, **(D)** rotorod test, **(E)** social interaction with a juvenile test, with initial testing and then again three days later. **(F)** fear conditioning cue test, **(G)** elevated plus maze, **(H)** prepulse inhibition, **(I)** Y-maze, and **(J)** indirect calorimetry using the Oxymax CLAM metabolic cage system. Data are shown for the entire cohort combining both sexes or divided into either male or female cohorts to examine sexual dimorphism in phenotype. Data represent the mean -/+ S.E.M., and statistically significant difference between *Taar5*$^{+/+}$ and *Taar5*$^{-/-}$ mice are denoted by * = $p<0.05$ and ** = $p<0.01$.

Figure 3. The Trimethylamine Receptor TAAR5 Shapes Circadian Oscillations in the Gut Microbiome. Male chow-fed wild type (*Taar5*$^{+/+}$) or mice lacking the TMA receptor (*Taar5*$^{-/-}$) were necropsied at 4-hour intervals to collect cecum for microbiome composition analyses via sequencing the V4 region of the 16S rRNA (genus level changes are shown). **(A)** Canonical correspondence analysis (CCA) based beta diversity analyses show distinct microbiome

compositions in *Taar5*$^{+/+}$ and *Taar5*$^{-/-}$ mice. Statistical significance and beta dispersion were estimated using PERMANOVA. **(B)** The relative abundance of cecal microbiota in *Taar5*$^{+/+}$ and *Taar5*$^{-/-}$ mice. Significantly altered cecal microbial genera in *Taar5*$^{+/+}$ and *Taar5*$^{-/-}$ mice are shown at ZT2 **(C)**, ZT6 **(D)**, ZT10 **(E)**, ZT14 **(F)**, ZT18 **(G)**, and ZT22 **(H)**. ASVs that were significantly different in abundance (MetagenomeSeq with Benjamini-Hochberg FDR multiple test correction, adjusted $p<0.01$). Data shown represent the means -/+ S.D. for n= 3-6 individual mice per group. Group differences were determined using ANOVA with Benjamini-Hochberg false discovery rate (FDR) multiple test correction, * = adjusted $p<0.01$).

Figure 3 – Figure Supplement 1. TAAR5-Deficient Mice Have Altered Circadian Oscillations in the Gut Microbiome. Male chow-fed wild type (*Taar5*$^{+/+}$) or mice lacking the TMA receptor (*Taar5*$^{-/-}$) were necropsied at 4-hour intervals to collect cecum for microbiome composition analyses via sequencing the V4 region of the 16S rRNA (genus level changes are shown). The relative abundance of cecal microbiota at the genus level are shown, and group differences were determined using cosinor analyses *p*-values are provided where there were statistically significant differences between *Taar5*$^{+/+}$ and *Taar5*$^{-/-}$ mice. The complete cosinor statistical analysis for circadian data can be found in Table S1. * = Significant differences between *Taar5*$^{+/+}$ and *Taar5*$^{-/-}$ mice by student's t-tests within each ZT time point ($p<0.05$).

Figure 4. Transplanting a Defined Synthetic Microbial Community With or Without Genetically Deleted Trimethylamine Production Capacity (*ΔcutC*) Alters Host Circadian Rhythms. Germ-free C57Bl/6 mice (recipients) were gavaged with the core community (*B. caccae, B. ovatus, B. thetaiotaomicron, C. aerofaciens, E. rectale*) with TMA producing wild type (WT) *C. sporogenes* (produces TMAO) or *C. sporogenes* Δ*cutC.* Gnotobiotic mice were then necropsied at 4-hour intervals to collect tissues including plasma (**A** and **C**) and olfactory bulb

(B). (A) Plasma choline, L-carnitine, betaine, γ-butyrobetaine, trimethylamine (TMA), and trimethylamine N-oxide (TMAO) were quantified by liquid chromatography with online tandem mass spectrometry (LC-MS/MS). (**B**) PCR was performed on olfactory bulb to examine key circadian clock regulators. **(C)** Plasma levels of select cytokines including interleukins (IL-1b, IL-2, and IL-33) and other plasma metabolites and hormones were measured as described in the methods section. Data shown represent the means -/+ S.E.M. for n= 5-6 individual mice per group. Differences between WT-*cutC* and Δ*cutC* groups were determined using cosinor analyses *p*-values are provided where there were statistically significant differences between group for circadian statistics. The complete cosinor statistical analysis for circadian data can be found in Table S1. Significant differences between WT-*cutC* and Δ*cutC* groups were also analyzed by student's t-tests within each ZT time point (* = $p<0.05$ and ** = $p<0.01$).

Figure 4 – Figure Supplement 1. Mice Lacking Either Gut Microbial TMA Production or Host-Driven TMA Oxidation Have Altered Circadian Rhythms. (A,B) Female germ-free C57Bl/6 mice (recipients) were gavaged with the core community (*B. caccae, B. ovatus, B. thetaiotaomicron, C. aerofaciens, E. rectale*) with TMA producing wild type (WT) *C. sporogenes* (produces TMAO) or *C. sporogenes* Δ*cutC.* Gnotobiotic mice were then necropsied at 4-hour intervals to collect tissues including subscapular brown adipose tissue **(A)** and plasma **(B).** Gene expression was quantified by qPCR and cytokines and metabolite levels were quantified as described in the method section. Data for panels B and C were analyzed by cosinor analyses and representative p-values are shown; The complete statistical analysis for circadian metrics can be found in Table S1. **(C)** Female wild type ($Fmo3^{+/+}$) or flavin-containing monooxygenase 3 knockout ($Fmo3^{-/-}$) mice were necropsied at ZT2 or ZT14 and TMAO levels were measured by LC-MS/MS and olfactory bulb circadian gene expression was quantified by qPCR. Data shown represent the means -/+ S.E.M. for n= 4-6 individual mice per group. Group differences were

determined using cosinor analyses *p*-values are provided where there were statistically significant differences between group for circadian statistics. The complete cosinor statistical analysis for circadian data can be found in Table S1. Significant differences between by student's t-tests within each ZT time point (* = $p<0.05$ and ** = $p<0.01$).

Table S1. Cosinor analyses for all circadian data include in this manuscript.

FIGURE 1

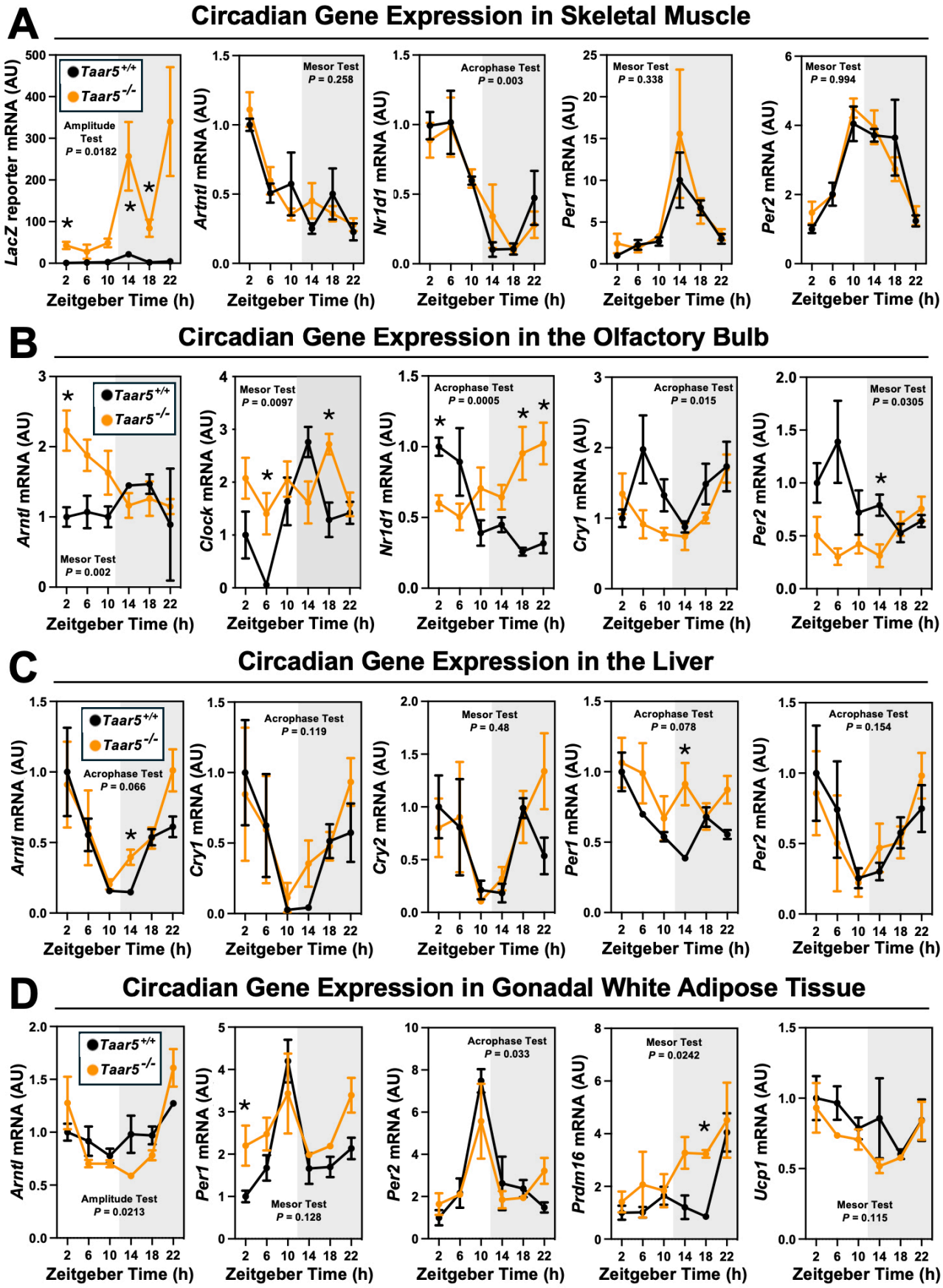
A
Circadian Gene Expression in Skeletal Muscle
Taar5+/+
Taar5-/-
Amplitude Test P = 0.0182
LacZ reporter mRNA (AU)
Mesor Test P = 0.258
Arntl mRNA (AU)
Acrophase Test P = 0.003
Nr1d1 mRNA (AU)
Mesor Test P = 0.338
Per1 mRNA (AU)
Mesor Test P = 0.994
Per2 mRNA (AU)
Zeitgeber Time (h)
B
Circadian Gene Expression in the Olfactory Bulb
Arntl mRNA (AU)
Mesor Test P = 0.002
Mesor Test P = 0.0097
Clock mRNA (AU)
Acrophase Test P = 0.0005
Nr1d1 mRNA (AU)
Acrophase Test P = 0.015
Cry1 mRNA (AU)
Mesor Test P = 0.0305
Per2 mRNA (AU)
C
Circadian Gene Expression in the Liver
Acrophase Test P = 0.066
Arntl mRNA (AU)
Acrophase Test P = 0.119
Cry1 mRNA (AU)
Mesor Test P = 0.48
Cry2 mRNA (AU)
Acrophase Test P = 0.078
Per1 mRNA (AU)
Acrophase Test P = 0.154
Per2 mRNA (AU)
D
Circadian Gene Expression in Gonadal White Adipose Tissue
Amplitude Test P = 0.0213
Arntl mRNA (AU)
Mesor Test P = 0.128
Per1 mRNA (AU)
Acrophase Test P = 0.033
Per2 mRNA (AU)
Mesor Test P = 0.0242
Prdm16 mRNA (AU)
Mesor Test P = 0.115
Ucp1 mRNA (AU)

FIGURE 1 – FIGURE SUPPLEMENT 1

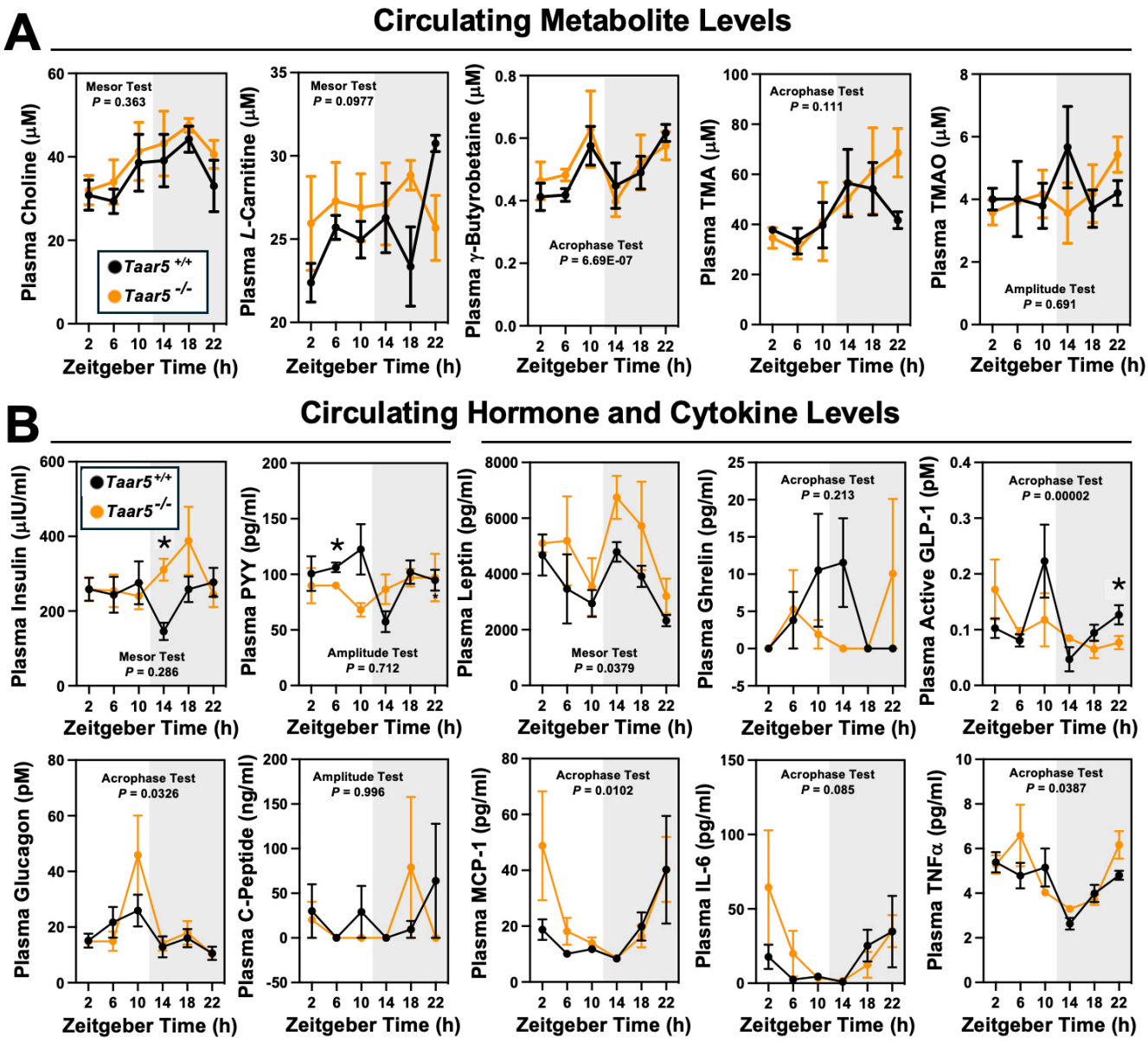

FIGURE 2

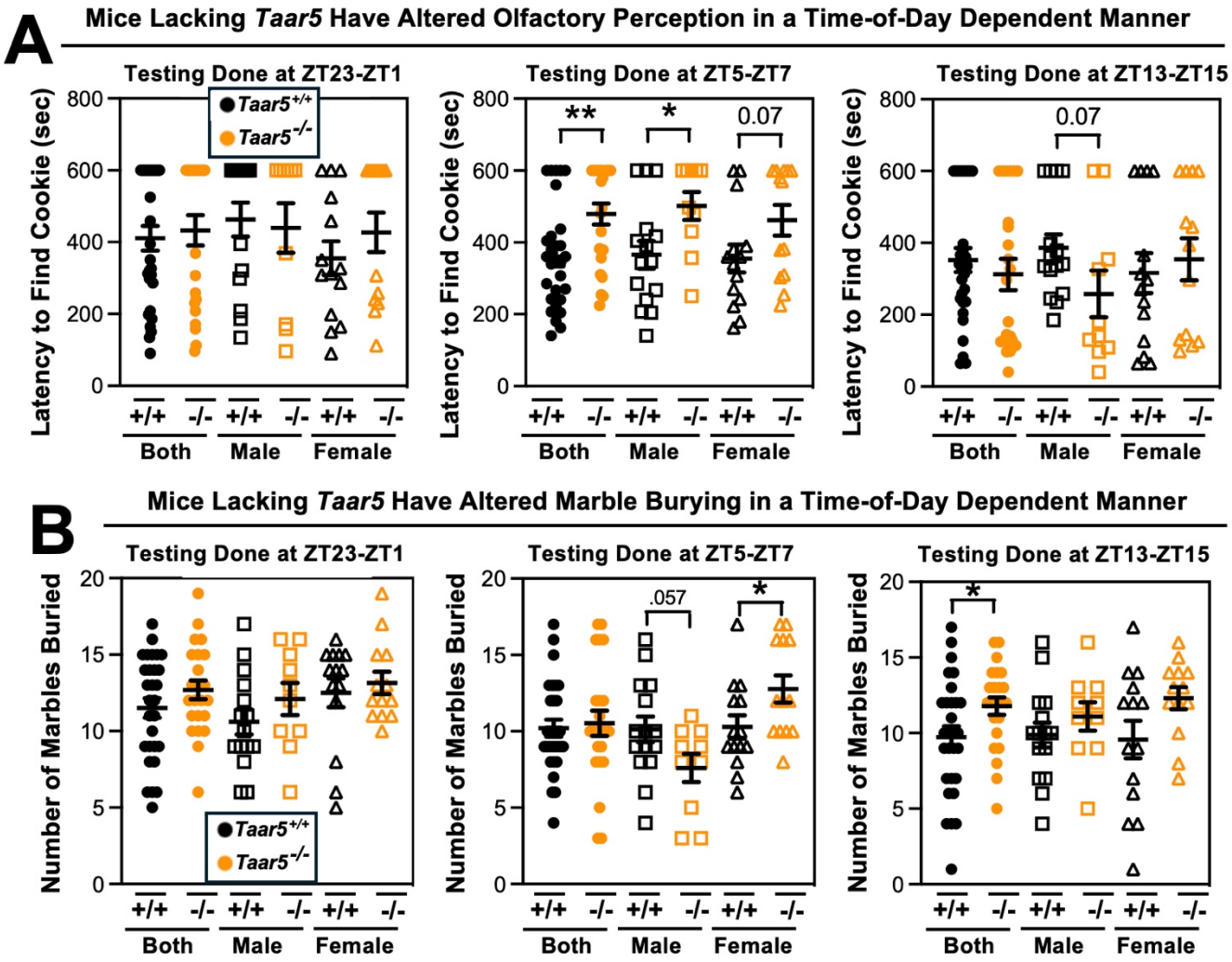
A
Mice Lacking Taar5 Have Altered Olfactory Perception in a Time-of-Day Dependent Manner
Testing Done at ZT23-ZT1
Testing Done at ZT5-ZT7
Testing Done at ZT13-ZT15
Latency to Find Cookie (sec)
Taar5+/+
Taar5-/-
**
*
0.07
+/+ -/- +/+ -/- +/+ -/-
Both Male Female
B
Mice Lacking Taar5 Have Altered Marble Burying in a Time-of-Day Dependent Manner
Number of Marbles Buried
.057

FIGURE 2 – FIGURE SUPPLEMENT1

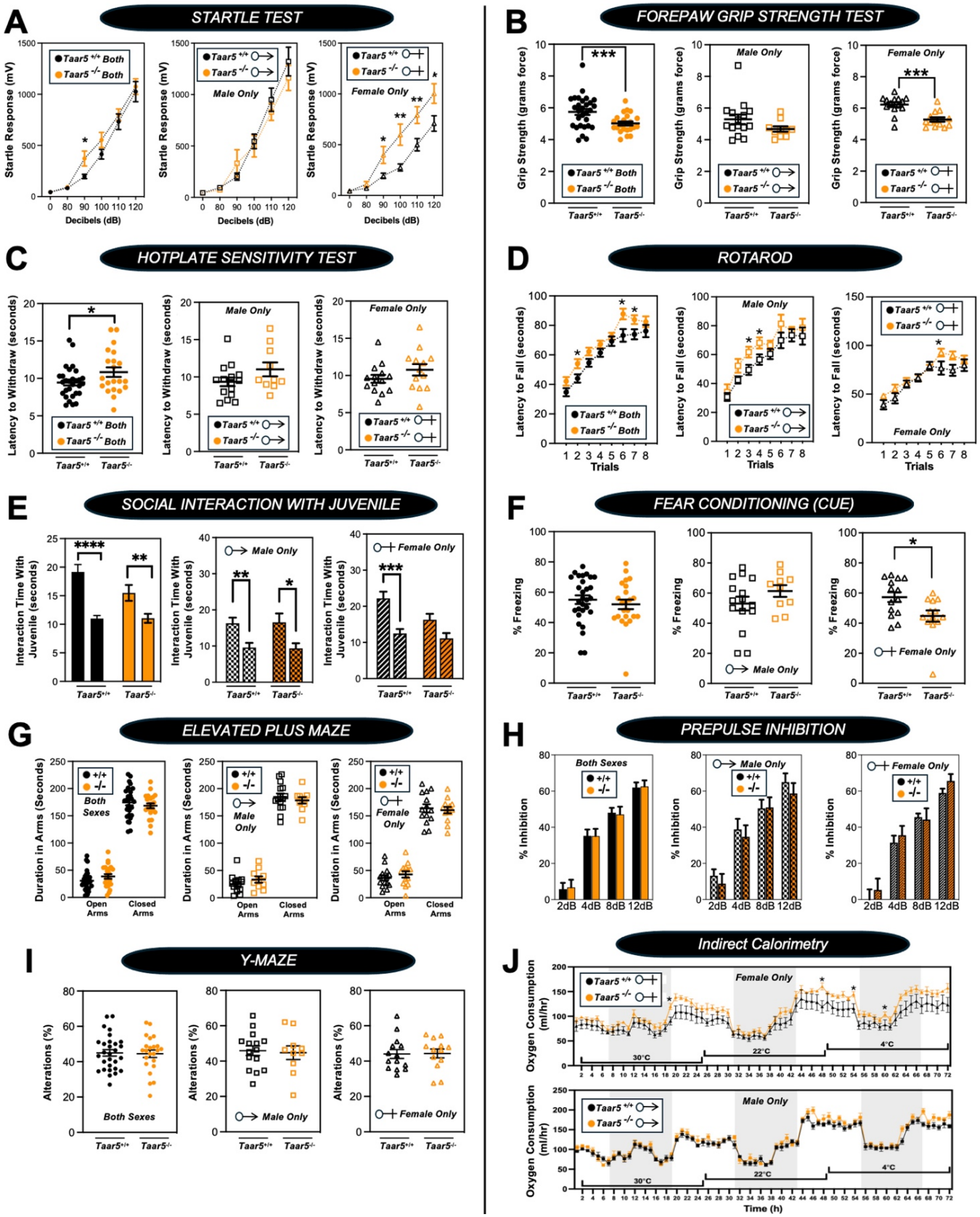

FIGURE 3

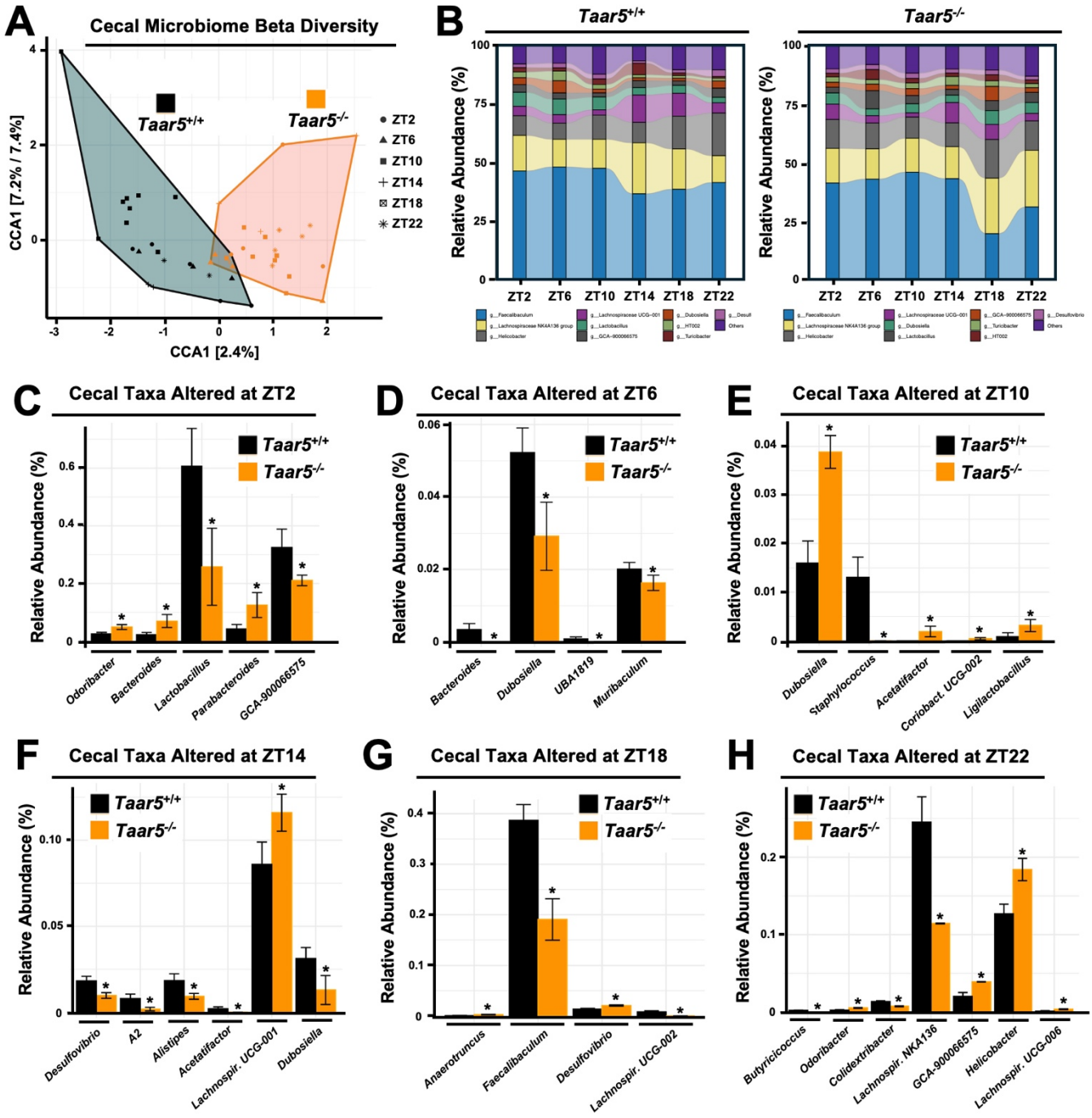
A
Cecal Microbiome Beta Diversity
Taar5+/+
Taar5-/-
ZT2
ZT6
ZT10
ZT14
ZT18
ZT22
CCA1 [7.2% / 7.4%]
CCA1 [2.4%]
B
Taar5+/+
Taar5-/-
Relative Abundance (%)
ZT2 ZT6 ZT10 ZT14 ZT18 ZT22
C
Cecal Taxa Altered at ZT2
Odoribacter
Bacteroides
Lactobacillus
Parabacteroides
GCA-900066575
D
Cecal Taxa Altered at ZT6
Bacteroides
Dubosiella
UBA1819
Muribaculum
E
Cecal Taxa Altered at ZT10
Dubosiella
Staphylococcus
Acetatifactor
Coriobact. UCG-002
Ligilactobacillus
F
Cecal Taxa Altered at ZT14
Desulfovibrio
A2
Alistipes
Acetatifactor
Lachnospir. UCG-001
Dubosiella
G
Cecal Taxa Altered at ZT18
Anaerotruncus
Faecalibaculum
Desulfovibrio
Lachnospir. UCG-002
H
Cecal Taxa Altered at ZT22
Butyricicoccus
Odoribacter
Colidextribacter
Lachnospir. NK4A136
GCA-900066575
Helicobacter
Lachnospir. UCG-006

FIGURE 3 – FIGURE SUPPLEMENT 1

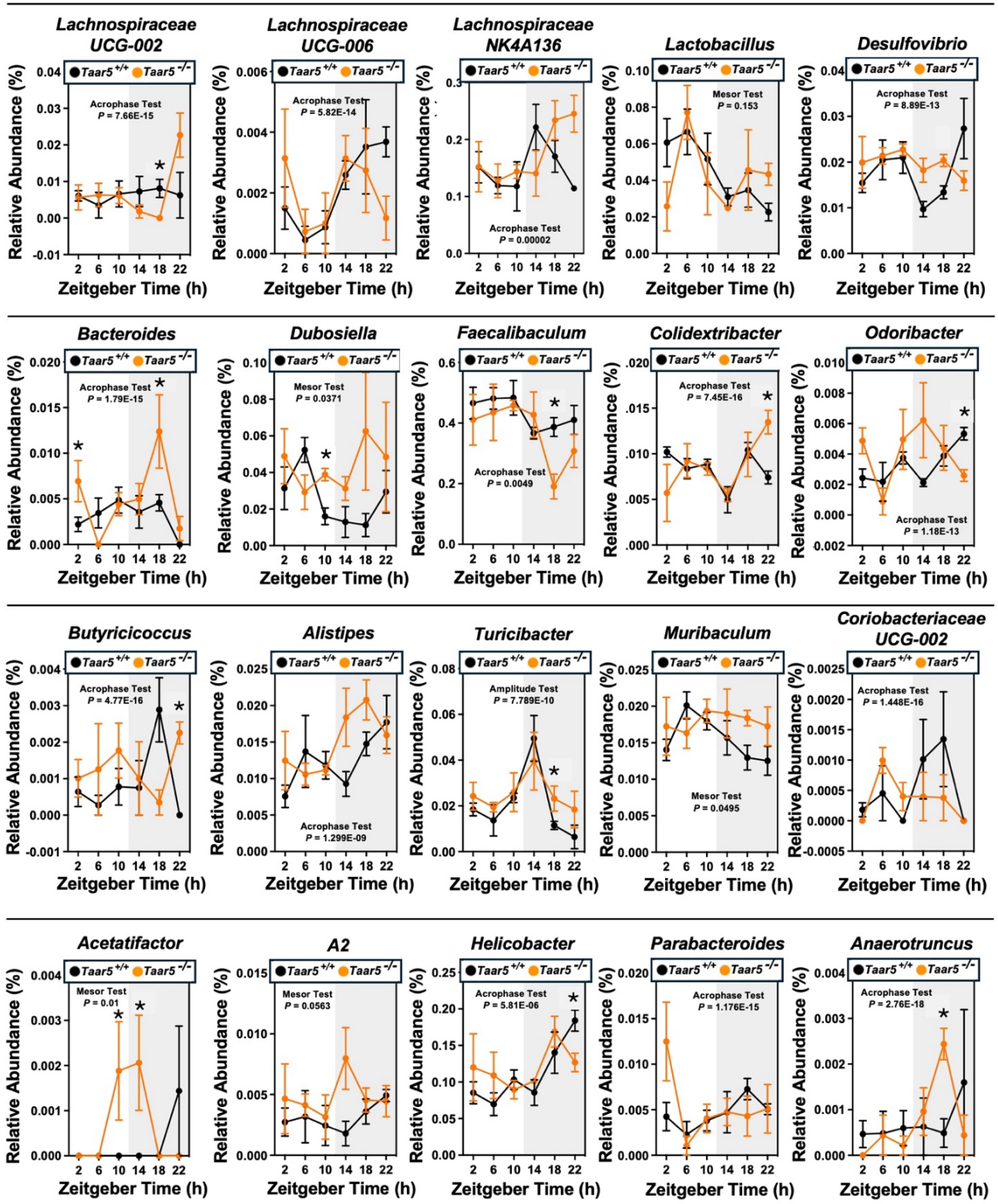

FIGURE 4

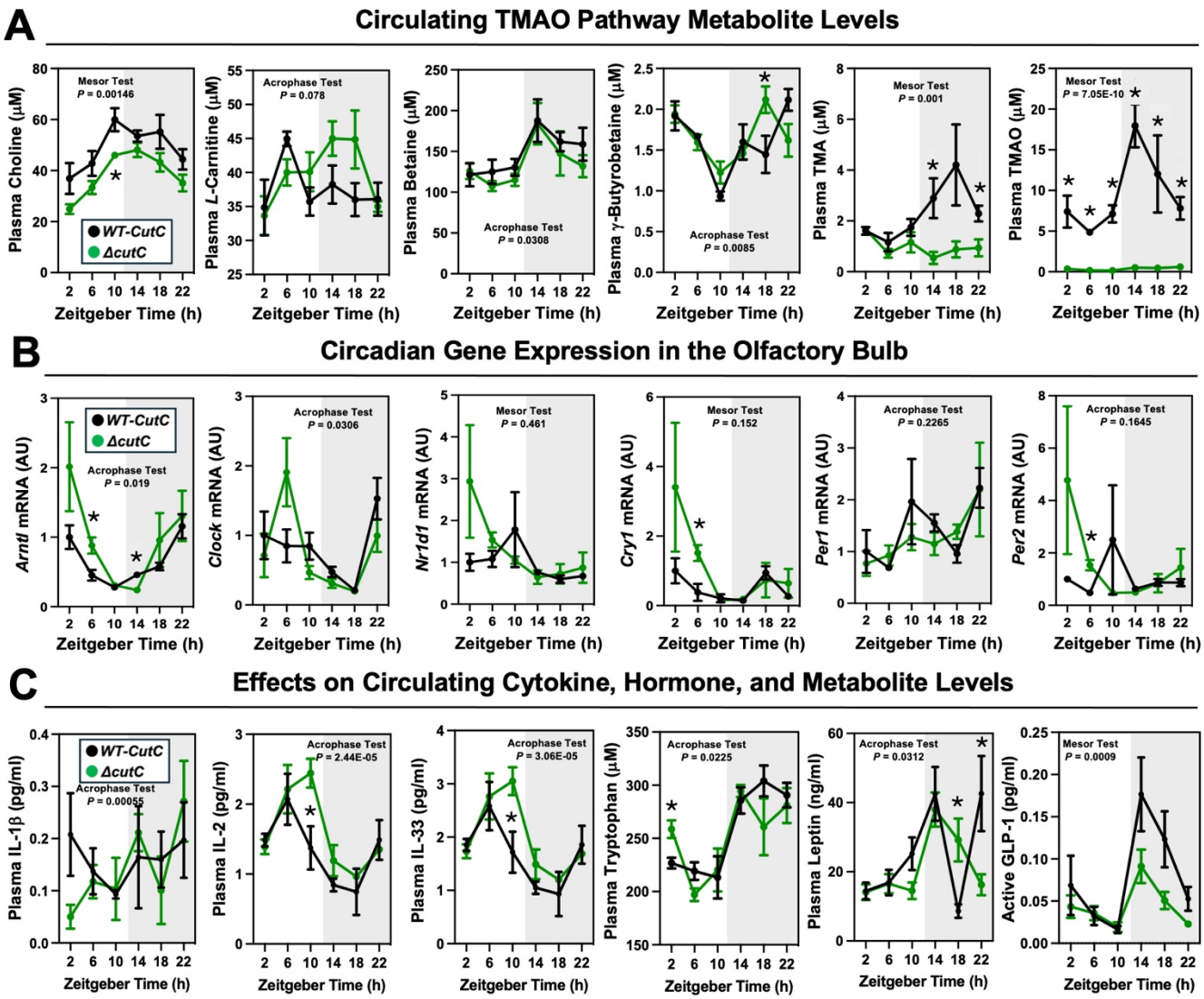
A
Circulating TMAO Pathway Metabolite Levels
Plasma Choline (μM)
Mesor Test
P = 0.00146
WT-CutC
ΔcutC
Plasma L-Carnitine (μM)
Acrophase Test
P = 0.078
Plasma Betaine (μM)
Acrophase Test
P = 0.0308
Plasma γ-Butyrobetaine (μM)
Acrophase Test
P = 0.0085
Plasma TMA (μM)
Mesor Test
P = 0.001
Plasma TMAO (μM)
Mesor Test
P = 7.05E-10
Zeitgeber Time (h)
B
Circadian Gene Expression in the Olfactory Bulb
Arntl mRNA (AU)
WT-CutC
ΔcutC
Acrophase Test
P = 0.019
Clock mRNA (AU)
Acrophase Test
P = 0.0306
Nr1d1 mRNA (AU)
Mesor Test
P = 0.461
Cry1 mRNA (AU)
Mesor Test
P = 0.152
Per1 mRNA (AU)
Acrophase Test
P = 0.2265
Per2 mRNA (AU)
Acrophase Test
P = 0.1645
Zeitgeber Time (h)
C
Effects on Circulating Cytokine, Hormone, and Metabolite Levels
Plasma IL-1β (pg/ml)
WT-CutC
ΔcutC
Acrophase Test
P = 0.00055
Plasma IL-2 (pg/ml)
Acrophase Test
P = 2.44E-05
Plasma IL-33 (pg/ml)
Acrophase Test
P = 3.06E-05
Plasma Tryptophan (μM)
Acrophase Test
P = 0.0225
Plasma Leptin (ng/ml)
Acrophase Test
P = 0.0312
Active GLP-1 (pg/ml)
Mesor Test
P = 0.0009
Zeitgeber Time (h)

FIGURE 4 – FIGURE SUPPLEMENT 1

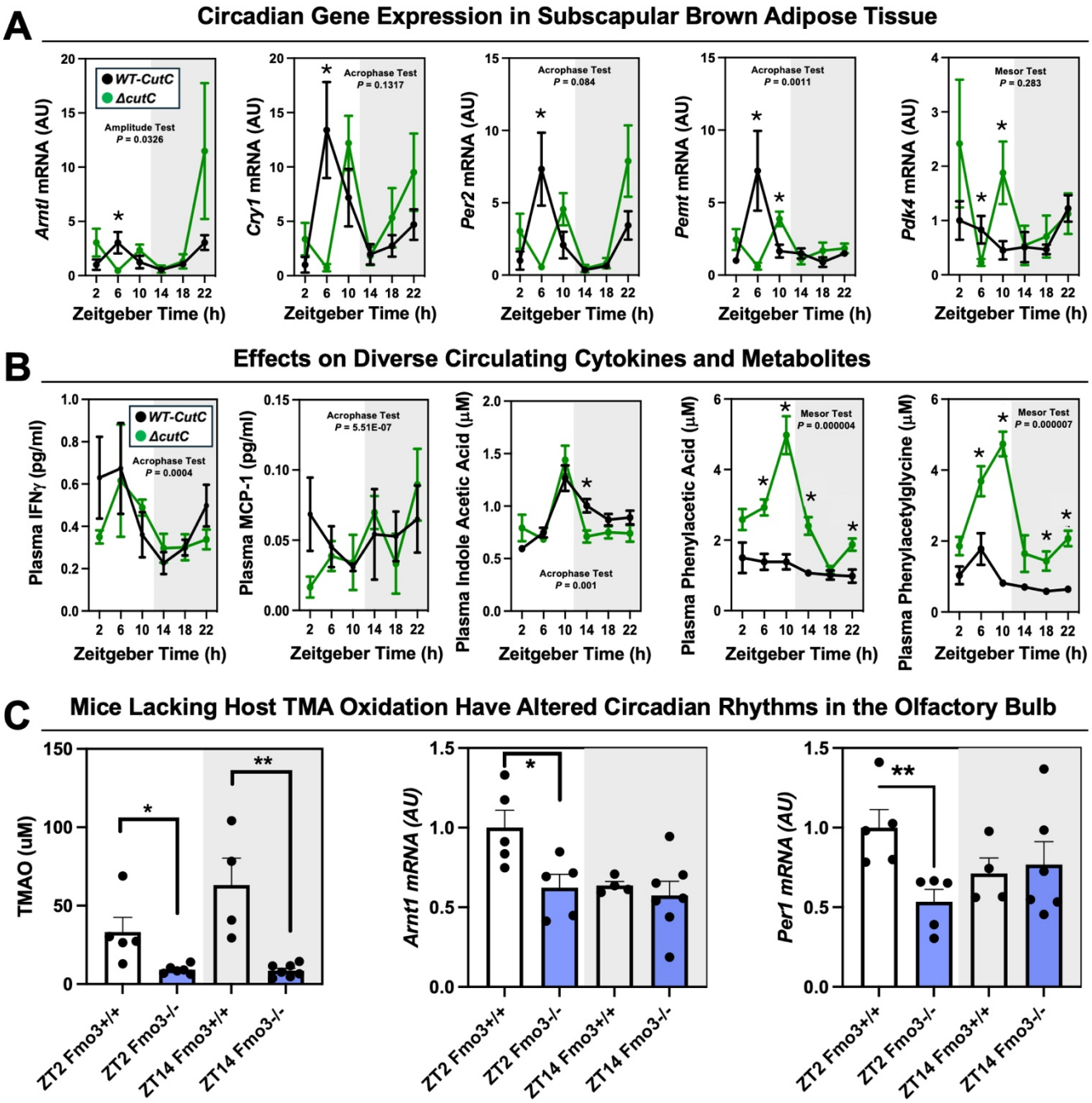

SUPPLEMENTAL TABLE 1. Cosinor analyses for all circadian timepoint studies.

	Gene	Group	Zero Amplitude Test	MESOR	Amplitude	Acrophase	Mesor Test	Amplitude Test	Acrophase Test
Figure 1A: Skeletal Muscle Gene Expression	*LacZ*	Taar5 +/+	**1.82E-02**	4.754 ± 24.113	9.899 ± 33.683	0.601 ± 6.688	**2.85E-04**	**1.82E-02**	2.58E-01
		Taar5-/-	1.19E-01	141.511 ± 34.834	251.811 ± 35.373	-1.23 ± 0.327			
	Arnt1	Taar5 +/+	6.53E-02	0.555 ± 0.062	0.796 ± 0.086	0.82 ± 0.368	2.58E-01	8.30E-01	1.61E-01
		Taar5-/-	**2.84E-02**	0.497 ± 0.089	0.735 ± 0.098	0.981 ± 0.36			
	Nr1d1	Taar5 +/+	**1.24E-07**	0.553 ± 0.048	1.072 ± 0.066	1.126 ± 0.132	3.79E-01	6.28E-01	**2.76E-03**
		Taar5-/-	**6.09E-05**	0.521 ± 0.069	0.961 ± 0.074	1.445 ± 0.153			
	Per1	Taar5 +/+	**6.67E-05**	4.129 ± 0.987	7.785 ± 1.37	0.954 ± 0.388	3.38E-01	6.53E-01	2.10E-01
		Taar5-/-	5.31E-02	5.215 ± 1.426	10.66 ± 1.547	0.819 ± 0.252			
	Per2	Taar5 +/+	**1.45E-04**	2.679 ± 0.198	4.415 ± 0.278	0.347 ± 0.161	9.94E-01	6.54E-01	1.03E-01
		Taar5-/-	**2.26E-07**	2.708 ± 0.286	4.364 ± 0.285	0.05 ± 0.182			
Figure 1B: Olfactory Bulb Gene Expression	*Arnt1*	Taar5 +/+	1.26E-01	1.167 ± 0.086	1.408 ± 0.117	1.155 ± 0.526	**2.44E-03**	6.28E-01	8.57E-02
		Taar5-/-	**1.12E-02**	1.523 ± 0.127	2.027 ± 0.142	1.321 ± 0.249			
	Clock	Taar5 +/+	**2.71E-02**	1.332 ± 0.162	2.065 ± 0.226	0.832 ± 0.318	**9.77E-03**	3.13E-01	**1.92E-02**
		Taar5-/-	5.56E-01	1.883 ± 0.243	2.134 ± 0.274	1.197 ± 0.955			
	Nr1d1	Taar5 +/+	**1.23E-04**	0.556 ± 0.052	0.93 ± 0.072	1.006 ± 0.198	**1.74E-02**	7.88E-01	**5.11E-04**
		Taar5-/-	**3.46E-02**	0.755 ± 0.077	0.984 ± 0.08	-1.193 ± 0.364			
	Cry1	Taar5 +/+	9.27E-01	1.372 ± 0.108	1.443 ± 0.15	1.032 ± 2.197	1.61E-01	5.40E-01	**1.51E-02**
		Taar5-/-	**1.00E-03**	1.104 ± 0.162	1.575 ± 0.162	-0.201 ± 0.385			
	Per2	Taar5 +/+	**4.14E-02**	0.829 ± 0.072	1.16 ± 0.1	1.373 ± 0.31	**3.05E-02**	6.25E-01	**7.66E-03**
		Taar5-/-	**2.17E-02**	0.498 ± 0.107	0.697 ± 0.106	-0.699 ± 0.61			
Figure 1C: Liver Gene Expression	*Arnt1*	Taar5 +/+	**5.81E-03**	0.519 ± 0.076	0.936 ± 0.102	0.182 ± 0.273	9.84E-01	6.46E-01	6.64E-02
		Taar5-/-	**2.56E-03**	0.614 ± 0.112	1.006 ± 0.113	-0.075 ± 0.304			
	Cry1	Taar5 +/+	**1.15E-02**	0.471 ± 0.099	0.951 ± 0.132	0.183 ± 0.309	9.67E-01	6.30E-01	1.19E-01
		Taar5-/-	**2.06E-02**	0.552 ± 0.143	0.945 ± 0.141	-0.06 ± 0.391			
	Cry2	Taar5 +/+	3.52E-01	0.877 ± 0.248	1.504 ± 0.351	1.018 ± 0.56	7.41E-01	4.80E-01	1.54E-01
		Taar5-/-	4.72E-01	0.88 ± 0.363	1.186 ± 0.361	-0.053 ± 1.283			
	Per1	Taar5 +/+	**3.82E-03**	0.669 ± 0.051	0.909 ± 0.069	0.507 ± 0.313	1.23E-01	5.31E-01	7.81E-02
		Taar5-/-	3.24E-01	0.862 ± 0.074	0.999 ± 0.08	0.781 ± 0.541			
	Per2	Taar5 +/+	**2.80E-02**	0.602 ± 0.086	0.979 ± 0.116	0.203 ± 0.344	6.76E-01	6.12E-01	1.54E-01
		Taar5-/-	**1.20E-02**	0.594 ± 0.125	0.947 ± 0.121	-0.207 ± 0.386			
Figure 1D: Subdural White Adipose Tissue Gene Expression	*Arnt1*	Taar5 +/+	5.01E-02	0.957 ± 0.052	1.114 ± 0.076	-0.5 ± 0.46	7.46E-01	**2.13E-02**	**2.14E-02**
		Taar5-/-	**2.70E-04**	1 ± 0.078	1.468 ± 0.074	-0.222 ± 0.197			
	Per1	Taar5 +/+	**1.53E-03**	2.093 ± 0.241	3.37 ± 0.35	-0.199 ± 0.258	1.28E-01	8.66E-01	6.56E-02
		Taar5-/-	9.96E-01	2.825 ± 0.358	2.857 ± 0.331	-0.585 ± 13.132			
	Per2	Taar5 +/+	**5.72E-05**	3.044 ± 0.433	5.964 ± 0.629	-0.217 ± 0.203	4.39E-01	9.09E-01	**3.32E-02**
		Taar5-/-	3.74E-01	3.164 ± 0.642	4.201 ± 0.612	-0.218 ± 0.732			
	Prdm16	Taar5 +/+	7.83E-01	1.388 ± 0.321	1.609 ± 0.46	-0.733 ± 2.018	**2.42E-02**	3.88E-01	**6.89E-03**
		Taar5-/-	1.25E-01	2.842 ± 0.476	4.218 ± 0.509	-1.292 ± 0.373			
	Ucp1	Taar5 +/+	6.30E-02	0.822 ± 0.048	1.003 ± 0.066	1.065 ± 0.385	1.15E-01	9.64E-01	3.39E-01
		Taar5-/-	7.15E-02	0.733 ± 0.072	0.908 ± 0.082	0.564 ± 0.404			
Figure S1A: Circulating Metabolites	*Plasma Choline*	Taar5 +/+	**4.90E-02**	36.34 ± 1.937	43.346 ± 2.69	0.955 ± 0.397	3.63E-01	9.33E-01	1.28E-01
		Taar5-/-	1.25E-01	39.974 ± 2.855	47.106 ± 3.279	1.047 ± 0.383			
	Plasma L-Carnitine	Taar5 +/+	8.53E-01	24.784 ± 0.781	25.398 ± 1.085	0.467 ± 1.832	9.77E-02	7.70E-01	5.40E-01
		Taar5-/-	8.06E-01	26.771 ± 1.17	27.576 ± 1.242	0.338 ± 1.563			
	Plasma γ-Butyrobetaine	Taar5 +/+	5.02E-01	0.49 ± 0.029	0.53 ± 0.04	0.898 ± 1.027	6.30E-01	7.86E-01	**6.70E-07**
		Taar5-/-	9.76E-01	0.528 ± 0.043	0.539 ± 0.045	-1.289 ± 4.027			
	Plasma TMA	Taar5 +/+	5.33E-02	43.982 ± 3.752	54.949 ± 5.213	1.226 ± 0.491	4.46E-01	5.55E-01	1.11E-01
		Taar5-/-	**4.73E-02**	48.983 ± 5.53	67.433 ± 5.893	-1.358 ± 0.314			
	Plasma TMAO	Taar5 +/+	8.26E-01	4.139 ± 0.293	4.409 ± 0.41	0.554 ± 1.549	9.24E-01	6.91E-01	3.46E-01
		Taar5-/-	2.19E-01	4.124 ± 0.446	4.88 ± 0.454	-0.615 ± 0.657			
Figure S1B: Circulating Hormones & Cytokines	*Plasma Insulin*	Taar5 +/+	6.30E-01	247.888 ± 17.712	272.029 ± 24.564	0.482 ± 1.057	2.86E-01	7.20E-01	2.67E-01
		Taar5-/-	1.97E-01	276.739 ± 26.221	331.367 ± 29.375	1.213 ± 0.47			
	Plasma PYY	Taar5 +/+	5.41E-01	99.806 ± 6.392	111.17 ± 9.13	-1.56 ± 0.788	4.42E-01	7.12E-01	3.29E-01
		Taar5-/-	3.43E-01	87.449 ± 9.463	99.271 ± 9.243	-0.614 ± 0.899			
	Plasma Leptin	Taar5 +/+	9.39E-01	3758.578 ± 368.525	3912.379 ± 520.425	-0.224 ± 3.393	**3.79E-02**	7.31E-01	5.29E-01
		Taar5-/-	5.79E-01	4704.115 ± 545.559	5435.666 ± 593.184	0.511 ± 0.758			
	Plasma Ghrelin	Taar5 +/+	**3.87E-02**	4.127 ± 2.019	10.62 ± 2.855	-0.268 ± 0.44	9.26E-01	6.46E-01	2.13E-01
		Taar5-/-	6.43E-01	3.689 ± 3.025	7.185 ± 3.102	-0.073 ± 0.944			
	Plasma Active GLP-1	Taar5 +/+	3.40E-01	0.119 ± 0.015	0.157 ± 0.022	-0.789 ± 0.56	5.27E-01	8.90E-01	**2.74E-05**
		Taar5-/-	2.40E-01	0.1 ± 0.022	0.135 ± 0.025	1.287 ± 0.642			
	Plasma Glucagon	Taar5 +/+	5.53E-02	17.512 ± 2.422	23.735 ± 3.481	-0.774 ± 0.541	8.05E-02	2.59E-01	**3.27E-02**
		Taar5-/-	**4.32E-02**	20.612 ± 3.585	32.869 ± 3.499	-0.468 ± 0.329			
	Plasma C-Peptide	Taar5 +/+	7.10E-01	22.174 ± 11.509	36.075 ± 16.111	0.014 ± 1.183	6.32E-01	9.96E-01	4.47E-01
		Taar5-/-	4.78E-01	14.894 ± 17.249	36.615 ± 18.463	-1.421 ± 0.831			
	Plasma MCP-1	Taar5 +/+	**3.48E-02**	17.669 ± 3.13	28.406 ± 4.473	-0.553 ± 0.408	3.39E-01	6.61E-01	**1.03E-02**
		Taar5-/-	**9.20E-03**	24.668 ± 4.633	43.882 ± 4.805	0.159 ± 0.257			
	Plasma IL-6	Taar5 +/+	**3.72E-02**	14.572 ± 4.767	30.045 ± 6.839	-0.689 ± 0.429	4.48E-01	6.88E-01	8.54E-02
		Taar5-/-	**1.99E-02**	22.187 ± 7.057	49.695 ± 7.476	0.309 ± 0.268			
	Plasma TNFα	Taar5 +/+	**3.32E-02**	4.554 ± 0.25	5.526 ± 0.349	0.965 ± 0.368	2.43E-01	4.84E-01	**3.88E-02**
		Taar5-/-	**4.59E-03**	4.898 ± 0.37	6.47 ± 0.405	0.584 ± 0.237			

	Gene		Group	Zero Amplitude Test	MESOR	Amplitude	Acrophase	Mesor Test	Amplitude Test
Figure S3: Gut-Microbial Oscillations	*Lachnospiraceae UCG-002*	Taar5 +/+	5.97E-01	0.006 ± 0.002	0.008 ± 0.002	1.396 ± 1.392	8.17E-01	6.95E-01	**7.67E-15**
		Taar5-/-	8.35E-02	0.008 ± 0.002	0.015 ± 0.002	-0.095 ± 0.37			
	Lachnospiraceae UCG-006	Taar5 +/+	**1.37E-02**	0.002 ± 0	0.004 ± 0.001	-1.315 ± 0.324	9.84E-01	5.01E-01	**5.83E-14**
		Taar5-/-	6.36E-01	0.002 ± 0.001	0.002 ± 0.001	1.46 ± 0.899			
	Lachnospiraceae NK4A136	Taar5 +/+	3.30E-01	0.151 ± 0.013	0.18 ± 0.018	1.349 ± 0.656	4.09E-01	5.61E-01	**2.43E-05**
		Taar5-/-	**1.13E-02**	0.177 ± 0.019	0.237 ± 0.019	-0.991 ± 0.349			
	Lactobacillus	Taar5 +/+	**4.33E-02**	0.047 ± 0.005	0.065 ± 0.007	1.416 ± 0.414	1.53E-01	8.31E-01	5.14E-01
		Taar5-/-	5.95E-01	0.042 ± 0.008	0.052 ± 0.009	1.258 ± 0.803			
	Desulfovibrio	Taar5 +/+	3.62E-01	0.017 ± 0.001	0.02 ± 0.002	1.312 ± 0.629	2.25E-01	9.14E-01	**8.89E-13**
		Taar5-/-	2.06E-01	0.02 ± 0.002	0.022 ± 0.002	-0.829 ± 0.802			
	Bacteroides	Taar5 +/+	1.27E-01	0.003 ± 0.001	0.005 ± 0.001	0.053 ± 0.658	8.12E-02	3.38E-01	**1.80E-15**
		Taar5-/-	1.50E-01	0.005 ± 0.001	0.008 ± 0.001	1.411 ± 0.35			
	Dubosiella	Taar5 +/+	**1.75E-02**	0.024 ± 0.006	0.04 ± 0.008	1.04 ± 0.538	**3.71E-02**	3.41E-01	**1.09E-07**
		Taar5-/-	6.40E-01	0.043 ± 0.009	0.054 ± 0.009	-0.947 ± 0.88			
	Faecalibaculum	Taar5 +/+	1.04E-01	0.435 ± 0.021	0.494 ± 0.029	1.521 ± 0.517	1.28E-01	4.70E-01	**4.97E-03**
		Taar5-/-	**2.03E-02**	0.374 ± 0.031	0.484 ± 0.032	-1.166 ± 0.303			
	Colidextribacter	Taar5 +/+	2.04E-01	0.009 ± 0.001	0.01 ± 0.001	0.043 ± 0.725	5.77E-01	5.24E-01	**7.46E-16**
		Taar5-/-	1.78E-01	0.009 ± 0.001	0.011 ± 0.001	-0.584 ± 0.47			
	Odoribacter	Taar5 +/+	3.48E-01	0.003 ± 0	0.004 ± 0.001	-1.482 ± 0.939	3.29E-01	7.73E-01	**1.18E-13**
		Taar5-/-	2.71E-01	0.004 ± 0.001	0.005 ± 0.001	0.626 ± 0.436			
	Butyricicoccus	Taar5 +/+	5.02E-02	0.001 ± 0	0.002 ± 0	1.475 ± 0.403	5.94E-01	6.72E-01	**4.78E-16**
		Taar5-/-	8.12E-01	0.001 ± 0	0.002 ± 0	0.616 ± 1.401			
	Alistipes	Taar5 +/+	5.71E-01	0.012 ± 0.001	0.014 ± 0.001	1.387 ± 0.909	1.23E-01	3.38E-01	**1.30E-09**
		Taar5-/-	**1.21E-02**	0.015 ± 0.002	0.02 ± 0.002	1.494 ± 0.309			
	Turicibacter	Taar5 +/+	**4.53E-02**	0.02 ± 0.003	0.03 ± 0.004	0.005 ± 0.382	1.57E-01	7.19E-01	**7.79E-10**
		Taar5-/-	3.36E-01	0.025 ± 0.004	0.032 ± 0.004	0.363 ± 0.609			
	Muribaculum	Taar5 +/+	**5.26E-03**	0.015 ± 0.001	0.019 ± 0.001	-0.921 ± 0.3	**4.95E-02**	5.29E-01	**2.37E-14**
		Taar5-/-	6.65E-01	0.018 ± 0.001	0.019 ± 0.001	0.463 ± 0.91			
	Coriobacteriaceae UCG-002	Taar5 +/+	1.51E-01	0.001 ± 0	0.001 ± 0	1.38 ± 0.423	2.81E-01	6.11E-01	**1.45E-16**
		Taar5-/-	1.23E-01	0 ± 0	0.001 ± 0	-0.737 ± 0.877			
	Acetatifactor	Taar5 +/+	3.19E-01	0 ± 0	0 ± 0	-0.586 ± 0.938	**1.00E-02**	8.33E-02	**4.02E-17**
		Taar5-/-	**1.92E-02**	0.001 ± 0	0.002 ± 0	0.039 ± 0.259			
	A2	Taar5 +/+	6.79E-01	0.003 ± 0.001	0.004 ± 0.001	-0.549 ± 1.096	5.63E-02	8.03E-01	**6.74E-10**
		Taar5-/-	5.48E-01	0.005 ± 0.001	0.006 ± 0.001	1.472 ± 0.794			
	Helicobacter	Taar5 +/+	**3.17E-02**	0.108 ± 0.009	0.144 ± 0.012	-1.283 ± 0.34	5.14E-01	9.05E-01	**5.81E-06**
		Taar5-/-	1.41E-01	0.117 ± 0.013	0.143 ± 0.013	-1.001 ± 0.539			
	Parabacteroides	Taar5 +/+	5.90E-02	0.005 ± 0.001	0.007 ± 0.001	-1.418 ± 0.551	5.54E-01	4.22E-01	**1.18E-15**
		Taar5-/-	2.64E-01	0.005 ± 0.001	0.008 ± 0.001	-0.022 ± 0.491			
	Anaerotruncus	Taar5 +/+	8.75E-01	0.001 ± 0	0.001 ± 0	-0.903 ± 1.74	8.81E-01	4.83E-01	**2.76E-18**
		Taar5-/-	**2.18E-02**	0.001 ± 0	0.002 ± 0	1.261 ± 0.302			
Figure 4A: Circulating Metabolites	*Plasma Choline*	WT-CutC	**5.24E-03**	48.996 ± 1.613	59.468 ± 2.293	0.405 ± 0.217	**1.46E-03**	7.74E-01	**9.62E-03**
		ΔCutC	**4.47E-07**	38.449 ± 2.182	49.649 ± 2.079	0.498 ± 0.186			
	Plasma L -Carnitine	WT-CutC	3.97E-01	37.502 ± 1.209	39.803 ± 1.709	-1.294 ± 0.743	3.91E-01	3.99E-01	7.81E-02
		ΔCutC	**7.91E-03**	39.771 ± 1.636	45.211 ± 1.558	0.511 ± 0.286			
	Plasma Betaine	WT-CutC	**1.79E-02**	147.098 ± 7.387	177.373 ± 10.633	1.228 ± 0.339	2.36E-01	9.60E-01	**3.08E-02**
		ΔCutC	**3.16E-02**	135.295 ± 9.995	163.756 ± 9.522	1.138 ± 0.335			
	Plasma γ-Butyrobetaine	WT-CutC	**8.38E-04**	1.605 ± 0.073	2.062 ± 0.102	-0.174 ± 0.229	6.75E-01	4.08E-01	**8.52E-03**
		ΔCutC	**1.28E-02**	1.66 ± 0.099	1.959 ± 0.094	-0.565 ± 0.314			
	Plasma TMA	WT-CutC	**1.41E-02**	2.315 ± 0.217	3.654 ± 0.312	1.415 ± 0.226	**1.48E-03**	3.21E-01	**7.76E-03**
		ΔCutC	2.03E-01	0.984 ± 0.294	1.298 ± 0.28	0.583 ± 0.894			
	Plasma TMAO	WT-CutC	**8.91E-03**	9.425 ± 0.694	14.543 ± 1	1.021 ± 0.188	**7.05E-10**	9.04E-02	**1.66E-05**
		ΔCutC	**3.78E-03**	0.378 ± 0.939	0.584 ± 0.894	-1.162 ± 4.339			
Figure 4B: Olfactory Bulb Gene Expression	*Arnt1*	WT-CutC	**1.29E-05**	0.655 ± 0.12	1.076 ± 0.169	-0.235 ± 0.401	1.28E-01	5.48E-01	**1.94E-02**
		ΔCutC	**1.29E-03**	0.951 ± 0.16	1.759 ± 0.151	0.129 ± 0.187			
	Clock	WT-CutC	5.92E-02	0.827 ± 0.124	1.214 ± 0.177	0.528 ± 0.447	6.89E-01	6.55E-01	**3.07E-02**
		ΔCutC	**6.50E-03**	0.766 ± 0.167	1.377 ± 0.159	1.117 ± 0.261			
	Nr1d1	WT-CutC	1.90E-01	0.998 ± 0.232	1.484 ± 0.325	-0.965 ± 0.684	4.61E-01	6.35E-01	1.64E-01
		ΔCutC	**4.22E-02**	1.294 ± 0.315	2.208 ± 0.3	0.842 ± 0.328			
	Cry1	WT-CutC	1.57E-01	0.49 ± 0.28	0.761 ± 0.391	-0.2 ± 1.484	1.52E-01	5.21E-01	1.70E-01
		ΔCutC	**3.82E-02**	1.105 ± 0.38	2.393 ± 0.362	0.589 ± 0.281			
	Per1	WT-CutC	7.50E-01	1.42 ± 0.203	1.657 ± 0.292	1.034 ± 1.188	4.31E-01	7.79E-01	2.27E-01
		ΔCutC	2.86E-01	1.283 ± 0.274	1.684 ± 0.261	-1.169 ± 0.652			
	Per2	WT-CutC	7.06E-01	1.095 ± 0.49	1.588 ± 0.679	-0.514 ± 1.435	5.52E-01	4.24E-01	1.65E-01
		ΔCutC	6.56E-02	1.594 ± 0.663	3.301 ± 0.632	0.477 ± 0.37			
Figure 4C: Circulating Cytokines, Hormones, & Metabolites	*Plasma IL-1β*	WT-CutC	5.63E-01	0.162 ± 0.027	0.205 ± 0.038	-0.36 ± 0.88	6.50E-01	8.98E-01	**5.59E-04**
		ΔCutC	1.95E-01	0.145 ± 0.037	0.217 ± 0.039	1.491 ± 0.464			
	Plasma IL-2	WT-CutC	**4.21E-03**	1.342 ± 0.102	1.936 ± 0.141	1.189 ± 0.25	9.45E-02	8.14E-01	**2.45E-05**
		ΔCutC	**5.82E-04**	1.562 ± 0.145	2.245 ± 0.152	-1.184 ± 0.202			
	Plasma IL-33	WT-CutC	**4.21E-03**	1.675 ± 0.128	2.417 ± 0.176	1.189 ± 0.25	9.45E-02	8.14E-01	**3.06E-05**
		ΔCutC	**5.82E-04**	1.95 ± 0.181	2.802 ± 0.19	-1.184 ± 0.202			
	Plasma Tryptophan	WT-CutC	**8.16E-06**	256.104 ± 7.029	307.892 ± 9.994	-1.45 ± 0.191	7.59E-01	6.53E-01	**2.25E-02**
		ΔCutC	**3.92E-03**	252.056 ± 9.511	290.166 ± 9.06	-1.382 ± 0.238			
	Plasma Leptin	WT-CutC	5.34E-01	25.035 ± 2.737	30.766 ± 3.944	1.006 ± 0.662	5.30E-01	4.47E-01	**3.12E-02**
		ΔCutC	**8.20E-04**	21.468 ± 3.734	32.134 ± 3.61	0.927 ± 0.335			
	Plasma Active GLP-1	WT-CutC	**1.55E-02**	0.076 ± 0.01	0.135 ± 0.014	1.272 ± 0.234	**9.63E-04**	4.56E-01	**1.23E-05**
		ΔCutC	1.00E-01	0.044 ± 0.014	0.063 ± 0.013	0.834 ± 0.685			

	Gene		Group	Zero Amplitude Test	MESOR	Amplitude	Acrophase	Mesor Test	Amplitude Test
Figure S4A: Brown Adipose Tissue Gene Expression	***Arnt1***	WT-CutC	1.80E-01	1.653 ± 0.958	2.44 ± 1.37	0.578 ± 1.703	2.39E-01	3.26E-01	1.76E-01
		ΔCutC	1.03E-01	3.207 ± 1.296	6.833 ± 1.235	-0.396 ± 0.341			
	Cry1	WT-CutC	6.33E-02	5.132 ± 1.197	9.024 ± 1.694	-1.326 ± 0.435	9.10E-01	3.75E-01	1.32E-01
		ΔCutC	8.66E-01	5.491 ± 1.62	6.374 ± 1.543	1.193 ± 1.749			
	Per2	WT-CutC	5.80E-02	2.436 ± 0.668	4.608 ± 0.962	1.272 ± 0.428	6.70E-01	7.99E-01	8.42E-02
		ΔCutC	2.02E-01	2.885 ± 0.904	4.606 ± 0.862	-0.126 ± 0.5			
	Pemt	WT-CutC	6.35E-02	2.222 ± 0.436	4.201 ± 0.622	-1.536 ± 0.309	4.09E-01	2.46E-01	**1.12E-03**
		ΔCutC	7.58E-01	1.925 ± 0.595	2.225 ± 0.581	-0.804 ± 1.881			
	Pdk4	WT-CutC	**3.82E-02**	0.747 ± 0.227	1.118 ± 0.321	0.2 ± 0.867	2.83E-01	9.45E-01	3.94E-01
		ΔCutC	5.39E-01	1.156 ± 0.31	1.587 ± 0.294	0.684 ± 0.701			
Figure S4B: Circulating Cytokines & Metabolites	***Plasma INF-γ***	WT-CutC	**1.91E-02**	0.451 ± 0.048	0.685 ± 0.067	0.84 ± 0.298	3.33E-01	5.40E-01	**4.36E-04**
		ΔCutC	1.09E-01	0.391 ± 0.068	0.531 ± 0.071	-1.349 ± 0.466			
	Plasma MCP-1	WT-CutC	5.63E-01	0.053 ± 0.009	0.068 ± 0.013	-0.36 ± 0.88	5.62E-01	5.09E-01	**5.52E-07**
		ΔCutC	1.95E-01	0.048 ± 0.012	0.071 ± 0.013	1.491 ± 0.464			
	Plasma Indole Acetic Acid	WT-CutC	**1.48E-03**	0.903 ± 0.052	1.145 ± 0.073	0.163 ± 0.306	2.08E-01	9.01E-01	**1.86E-03**
		ΔCutC	**3.94E-02**	0.853 ± 0.071	1.062 ± 0.067	-0.548 ± 0.322			
	Plasma Phenylacetic Acid	WT-CutC	1.51E-01	1.224 ± 0.149	1.49 ± 0.213	1.551 ± 0.783	**4.15E-06**	**2.35E-02**	**4.05E-03**
		ΔCutC	**1.06E-05**	2.654 ± 0.202	4.068 ± 0.192	-0.932 ± 0.136			
	Plasma Phenylacetylglycine	WT-CutC	**6.27E-03**	0.913 ± 0.166	1.388 ± 0.238	1.432 ± 0.488	**7.37E-06**	1.82E-01	**6.91E-05**
		ΔCutC	**6.54E-05**	2.573 ± 0.225	3.992 ± 0.214	-1.049 ± 0.151			